Research on a dielectric silicon lens antenna and an attenuator in the THz region

メタデータ	言語: en
	出版者: Shizuoka University
	公開日: 2015-12-16
	キーワード (Ja):
	キーワード (En):
	作成者: Catur, Apriono
	メールアドレス:
	所属:
URL	https://doi.org/10.14945/00009271

THESIS

Research on a dielectric silicon lens antenna and an attenuator in the THz region

CATUR   APRIONO

Department of Nanovision Technology

Graduate School of Science and Technology,

Educational Division, Shizuoka University

June 2015

ACKNOWLEDGMENTS

I confess that my journey to pursue Ph.D degree is not only caused by my own efforts, but also because supports and helps of other people who always encourage and facilitate me in this precious education process. In this moment, it is my pleasure to describe my gratitude to whose supports made me finish this thesis.

On the first occasion, I would like to express my profound gratitude to Professor Norihisa Hiromoto as my supervisor in the Department of Nanovision Technology, Graduate School of Science and Technology, Shizuoka University. I am thankful for useful discussion and encouragement during my research. Under guidance of Professor Hiromoto, I learned valuable experiences how to do critical thinking and proper research.

I would like to thanks deeply to Professor Eko Tjipto Rahardjo for supervising me since I was a Bachelor student in the Department of Electrical Engineering, Faculty of Engineering, Universitas Indonesia. Many advises, guidances and opportunities from Professor Eko Tjipto Rahardjo have brought me to pursue this Ph.D. program.

I would like to say thanks for Professor Djoko Hartanto from Department of Electrical Engineering, Faculty of Engineering, Universitas Indonesia who has initiated Double Degree Program (DDP) between Shizuoka University and Universitas Indonesia and also has suggested me to apply the DDP program and a scholarship from the Japanese Government Ministry of Education, Culture, Sports, Science and Technology (MEXT).

Also, I would like to say thank you very much to the official of the Department of Electrical Engineering, Faculty of Engineering, Universitas Indonesia, for fully supporting me to join the DDP, especially Dr. Muhamad Asvial (former head of the department) and Dr. Dodi Sudiana (former Secretary of the department).

Catur Apriono

ABSTRACT

Terahertz (THz) wave radiation, which lies between microwave and infrared, has attracted many researchers to explore its potentials and to develop the THz wave technology. Various studies have shown potentials of the THz wave applications to solve some issues, such as non-destructive inspection of concealed weapons, food examination, pharmaceutical examination, and analysis of DNA molecules. In the development of the THz wave technology, source and detector performance, speed of measurement and cost are some issues for extending the utilization of the THz waves. Among those issues, we study two optical elements in the THz region to improve performance of THz systems, which are dielectric silicon lens antenna for focusing and collimating beams of THz wave radiation and a glass for attenuating THz wave at frequency 250 GHz applied for a body scanner system.

An extended hemispherical silicon lens antenna is an attractive and a practical element used in a THz system to focus and collimate beams of THz wave radiation. By adjusting the extension length to the focal point and placing a detector or an emitter at around the focus, we can improve coupling efficiency of the THz system. Because linearly polarized radiation is ordinary in the THz system, a practical method to calculate a precise profile of power-flow density distribution of the polarized THz wave radiation is important to design a silicon lens antenna.

In optics, the ray-tracing is widely used to design lenses and to analyze optical systems. However, if we calculate the power-flow density distribution, the regular ray-tracing method is not enough to evaluate a correct power-flow density distribution because it does not take into account transmittances depending on angles of incidence at different positions on the spherical boundary of the Si-lens.

In this research, we propose a ray-tracing method combined with Fresnel's transmission to calculate the power-flow density distribution in a silicon lens antenna irradiated with linearly polarized THz wave. Fresnel's transmission is

included in the proposed method to cover accurate transmittance and polarization dependence of the THz wave radiation.

A material of the dielectric lens considered in this work is high resistivity silicon, which has a very low dispersion of refractive index and low absorption in the range of 0.3 – 2.5 THz. Therefore, the proposed method is applicable for calculating power-flow density distribution in the wide range of THz region.

We consider an extended hemispherical Si-lens antenna with radius of the hemisphere and length of the extension are two millimeters and one millimeter, respectively. A parallel beam of THz waves are travelling to the Si-lens antenna. When the rays pass through the hemisphere boundary, transmittance and refractive angle of every ray are calculated by using Fresnel's law of transmission and Snell's law of refraction, respectively. By tracing the transmitted rays inside the Si-lens, the power-flow density distributions are calculated by considering the rays' path and the transmittance of the transmitted rays.

We execute an electromagnetic (EM) simulation by using CST Microwave (MW) studio at frequency 1 THz for incoming radiation with a linear polarization to compare with and confirm the results of the proposed method. We also compare our method with a regular ray-tracing of an optical simulator of Zemax to clarify the difference between them.

The power-flow-density distribution calculated by the proposed method has a good agreement except for interference and diffraction with the result obtained by the electromagnetic wave simulator. The result was consistent with each other, though the EM simulation has effect of interference and diffraction, which are not considered in our proposed method.

The power transmittance estimated by the proposed method is 68.3% of the input radiation power; on the other hand the one estimated by the regular ray-tracing

is 70.0% of the value for normal incidence. This shows the proposed method is necessary for executing the precise calculations.

Our proposed method is so simple and reliable that it is useful for designing and evaluating THz optical systems using dielectric lens antennas. The evaluation of the power-flow density distribution by the ray-tracing method with Fresnel's transmission will contribute to designing optical elements like dielectric lens antennas in THz quasi-optical systems.

After the discussion of the proposed method to calculate the power-flow density distribution, we study attenuation characteristics of soda-lime glass at frequency 250 GHz. An attenuator is an important element used in a THz system to prevent saturated power detected by a detector. In this research, we propose a low cost material of an ordinary glass or also known as soda-lime glass to effectively attenuate power of THz waves.

We analyze attenuation of the soda-lime glass at frequency 250 GHz from measurement data by using a pyro detector and a body scanner system. The THz waves passed through the glass is measured to obtain the measurement data. Some samples of the glass with different thickness are used in the analysis. Statistical analysis of the least square method is conducted to calculate the attenuation factor. To include Fresnel's transmission and refraction affected by the THz wave polarization, refractive index of the glass is measured by using a transmission THz time domain spectroscopy.

The results show that the glass is a potential material used to attenuate the THz wave. The refractive index measurement shows that the refractive index of the glass has low dispersion between 0.2 – 1 THz, therefore, the glass can provide an attenuation element for a wide range frequency. The glass attenuation analyzed from the pyro detector measurement data are around 0.556 mm^{-1} and 0.4988 mm^{-1} when the analysis conducted without and with consider the Fresnel's factor, respectively. The attenuation analyzed from the body scanner measurement without

consider the Fresnel's factor is around 0.574 mm^{-1}, which is close to the pyro detector result. The results show that the glass is a potential and low cost material to reduce around half of THz wave power for every 1 mm.

CONTENTS

LIST OF FIGURES

LIST OF TABLES

CHAPTER 1
INTRODUCTION

1.1 Research background

Terahertz (THz) wave radiation, which lies between microwave and infrared or in the range 300 GHz to 10 THz, is in transition between the electronic domain and the photonic domain. Figure 1-1 shows the electromagnetic spectrum and the position of the THz wave region [1]. The microwave as well as the infrared has been explored and developed for a long time ago. In the electronics domain, we are already familiar with radio communication, radar or microwaves technology terms, such as high frequency or HF, very high frequency or VHF, and ultra high frequency or UHF. In the photonics domain, terms, such as visible, x-ray, gamma-ray, are also well known related with many established technology, such as optical communications, medical imaging and also astrophysics. However, the utilization of the THz waves is still under developed even though the frequency region has many potentials for many kind applications as well. Lack of appropriate equipment, especially THz wave source, is the main challenge of exploting the THz wave region [2]. However, since the presence of femtosecond laser and photoconductive antenna in the 1980's [3], many researchers have been interested to explore the THz wave for various applications.
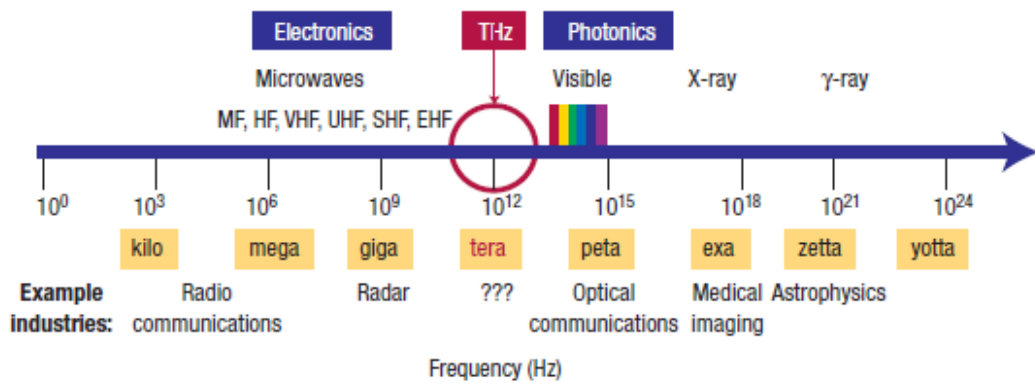
Figure 1-1The electromagnetic spectrum shows a THz gap between the electronics domain and the photonics domain **[1]**.

The THz wave has some attractive qualities, for example: it can yield extremely high-resolution images and move vast amounts of data quickly. It is non-ionizing meaning its photons are not energetic enough to knock electrons off atoms and molecules in human tissue, which could trigger harmful chemical reactions. The waves also stimulate molecular and electronic motions in many materials – reflection off some, propagating through others, and being absorbed by the rest [2]. At the THz waves, the absorption served as chemical fingerprints can be utilized to identify spesific or hazardous materials. These special characteristics have attracted many researchers to explore potentials of the THz wave and to develop THz technology. Various studies have been reported related to the development of THz technology for various applications, such as non-destructive inspection of concealed weapons [4], medical [5], food examination [6] [7] [8], pharmaceutical examination [9] [10], and analysis of DNA molecules [11]. Figure 1-2 shows the THz wave applications that have been reported by some researchers. In Figure 1-2 (a), the THz wave can reveal a concealed weapon in a suitcase for security applications [4]. Another study as shown in Figure 1-2 (b) shows a pharmaceutical examination of drugs [9]. The other advantage shown in Figure 1-2 (c) is a THz technology can conduct a non-destructive technique of a food inspection, which do not destroy the objects while the inspection being done [8].

(a)	(b)	(c)
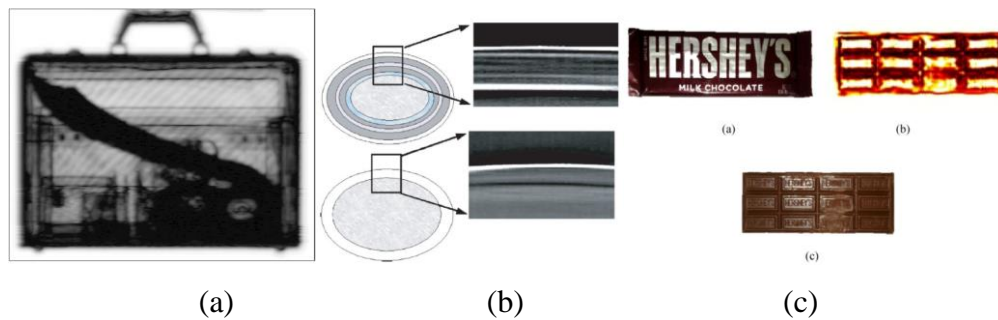
Figure 1-2 Some study of the THz waves applications for (a) inspection a concealed weapon **[4]**, (b) pharmaceutical examination **[9]**, and (c) non-destructive food inspection **[8]**.

The THz waves also have been studied and recommended to fulfill the demand for high data access in telecommunication systems [12]. The increasing carrier frequencies provided by the THz waves can be a solution to provide huge bandwidth for use in wireless communications. Although atmospheric attenuation in the THz wave frequency is larger than in the microwave frequency and poses a problem for using terahertz frequency for long-range communication and radar, the THz waves offers alternative for future wireless communications systems, especially for indoor applications such as WLANs and WPANs [13].

Although many reports have shown potentials of the development of THz technology, there are some critical issues to develop the THz technology for actual use, such as lack of appropriate source and detector performance, slow speed of measurement and high cost of devices necessary for marginal system [14]. An expected compact THz system should be powerful enough to overcome signal attenuation, efficient, affordable, and small enough or compact to be deployed practically in many fields. To make an affordable THz system, more researches are still needed to provide low cost and more practical techniques in developing THz systems. Among a lot of issues, in this work, we study two optical elements in the

THz waves region to improve performance of a THz system: a dielectric silicon lens antenna for focusing and collimating beams of THz wave radiation and a soda-lime glass as a low-cost THz wave attenuator for attenuating power of THz wave radiation.

In a device work at high frequencies such as the THz wave region, the silicon lens antenna is an effective solution to avoid total internal reflection for a THz wave source made on a finite dielectric substrate; therefore, it can solve the surface wave's problem. Because quasi-optical systems are ordinary applied in THz systems to reduce losses caused by diffraction effects, another advantage of the use of a silicon lens is able to improve the coupling efficiency of a THz wave source or a THz wave detector. By placing a THz wave detector, such as a THz bolometer detector or a THz antenna, in the focus of the silicon lens antenna, we can also improve its detectivity performance.

Study of the second element (the glass attenuator) is conducted to explore its optical characteristics as a THz wave attenuator to be implemented in a THz systems, such as 250 GHz radiation and body scanner system in this research. The use of the glass attenuator offers low cost material and practical technique to manipulate power of the THz waves radiation. The glass attenuator is a useful and practical elements to reduce the THz waves intensity to obtain optimum condition of the THz waves radiation applied in the THz system.

1.2 Materials for THz application

To design a THz element, we should consider an appropriate material works at the THz wave region. Optical characteristics of a material in the THz region are mostly different than in optics. Table 1-1 is a list of some potential materials for THz elements and their optical constant of refractive index (n), extinction index (k) and absorption coefficient (α) at frequency around 1 THz.

Table 1-1 Refractive index of several THz materials

at frequency around 1 THz

Materials	Refractive index (n)	Extinction coefficient (k)	Absorption Coefficient α (cm⁻¹)
High-resistivity Si [1]	3.4139	0.0001	0.04
Ge [15]	4.0052	0.00204	0.8549
Quartz (z-cut x-quartz) [2]	2.1011	0.0007	0.3012
ZnTe [16]	3.1854	0.00572	2.58
GaAs [17]	3.611	0.0014	0.5867
LiNbO3 [18]	6.70	0.0045	1.8857
GaP [19]	3.3399	0.00453	1.8983
Polyethylene (PE) [20]	1.51381	0.0040	1.6762
Teflon (PTFE) [21]	1.43		
Mylar (PET) [22]	1.712		
THz Super lens (Tsurupica ™) [23]	1.52		
Glass [3]	2.7152		

In design a dielectric lens, refractive index of a material is one consideration to focus or collimate THz beams. A high value of refractive index is necessary to focus effectively the THz waves by the dielectric lens. As listed in Table 1-1, there are some materials which have high value of refractive index, if we consider the refractive index higher than 3, such as high-resistivity silicon, Ge, ZnTe, GaAs, LiNbO3 and GaP.

---

[1] Obtained from transmission THz-TDS measurement
[2] Obtained from transmission THz-TDS measurement
[3] Obtained from transmission THz-TDS measurement

After we determine the materials with high refractive index, materials with low extinction coefficient (*k*) or also known as the imaginary part of the refractive index and absorption coefficient (α) are important to avoid losses when the THz waves propagating in the dielectric lens. As listed in Table 1-1, a high-resistivity silicon is the most appropriate material among those materials in order to make a THz dielectric lens antenna.

We measure refractive index and absorption coefficient of the high-resistivity silicon in the THz range for THz elements by using THz Time Domain Spectroscopy (TDS) to verify its potential. Figure 1-3 shows that refractive index of the high resistivity silicon has a low dipersion in the THz range (about 0.3 – 4 THz). Another measurement of a silicon by other group also shows comparable results in the THz range [24]. This characteristic is useful to design a wide band THz element. Absorption coefficient of the high resistivity silicon as shown in Figure 1-4 shows that the material has low absorption coefficient not only at single frequency as listed in Table 1-1 but also in the THz range.
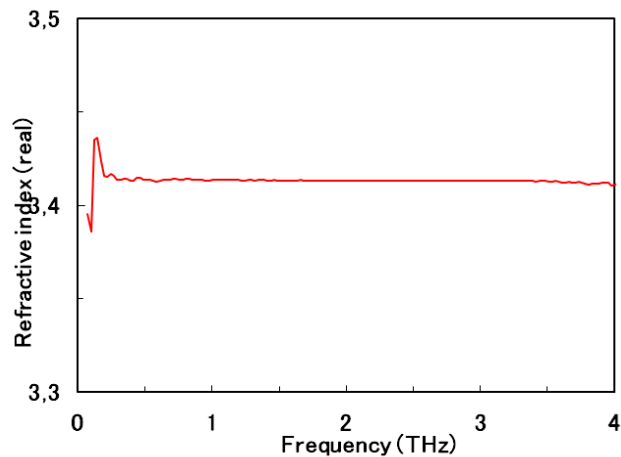
Figure 1-3 Refractive index of High-resistivity silicon measured with THz Time Domain Spectroscopy (TDS) in the THz region[4].

---

[4] Obtained from transmission THz-TDS measurement
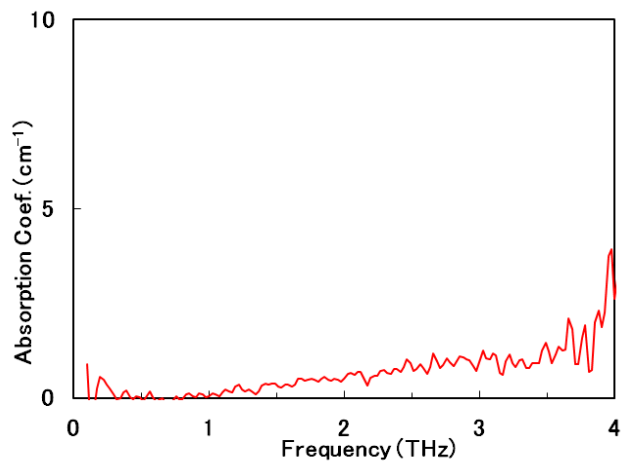
Figure 1-4 Absorption coefficient of High-resistivity silicon measured with THz Time Domain Spectroscopy (TDS) in the THz region[5].

Another variable that should be considered to design the THz optical element is resistivity (or conductivity) of materials. High-resistivity materials are necessary to avoid free carrier absorption or to obtain low losses when THz waves propagating in those materials. Resistivity of materials for THz applications are affected by impurity concentration. For comparison of the resistivity affected by the impurity concentration, Figure 1-5 (a) and (b) show resistivity characteristics of silicon and GaAs as a function of impurity concentration, respectively [25]. Figure 1-5 shows that the higher resistivity of both materials are obtained when the lower impurity concentration. At room temperature, the resistivity of silicon as shown in Figure 1-5 (a) is higher than GaAs as shown in Figure 1-5 (b). By using the high-resistivity silicon, which has very low absorption coefficient and high resistivity, we can consider only the real part of the refractive index to design a dielectric lens applied for a THz system.

---

[5] Obtained from transmission THz-TDS measurement
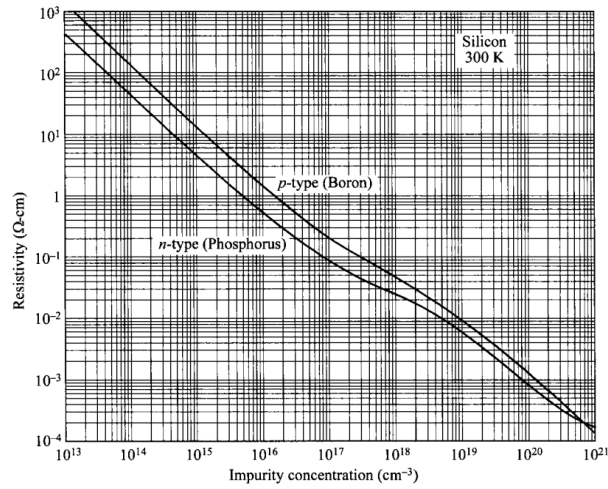
(a)
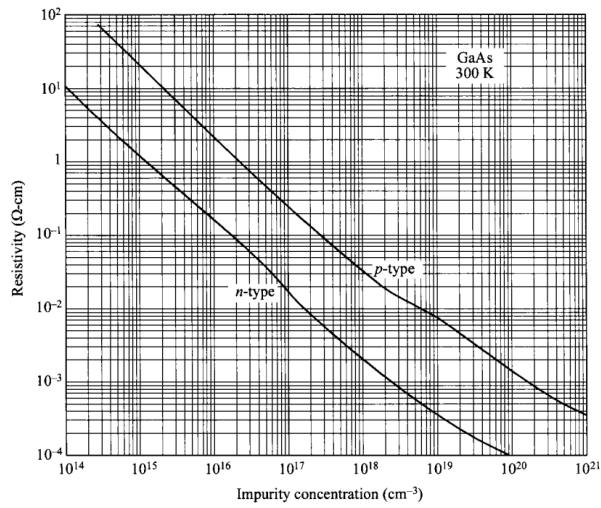
(b)

Figure 1-5 Resistivity versus impurity concentration at temperature 300 K for (a) silicon and (b) GaAs **[25]**

The high-resistivity, the low dispersion of the high refractive index and the low absorption coefficient in the wide THz range shows that the high-resistivity silicon is a good candidate material for designing a THz dielectric lens antenna to obtain effective focusing of THz beams into THz elements (THz wave detecting or transmitting elements) in a wide range of the THz region.

1.3 Quasi-optical in THz systems

In optics, wavelength of electromagnetic radiation is small compared to size of the optical components, therefore, the diffraction effect can be ignored. Geometrical optics is a relevant method to characterize the optical elements. For frequencies lower than optics where the wavelength is probably becoming comparable to the size of the optical elements, the diffraction effect become significant.

Methods of propagation, such as coaxial cables, micro strip, strip line, and slot line, are ordinary applied at radio and microwave frequencies, which almost single-mode systems. But, losses increases at higher frequencies. On the other hand, we may consider the lossless of the electromagnetic propagation in free space. However, any system that would satisfy the optical condition would be impractical for a relatively large wavelength [26].

In THz systems, quasi-optical systems are ordinary applied as consideration of the electromagnetic radiation wavelength. In order to solve the diffraction effect, a coupling element, such as a dielectric lens, is used to couple the free space electromagnetic propagation into a THz elements or vice versa. The dielectric lens focuses the incoming radiation into a THz wave detector or collimate the emitted radiation from a THz wave emitter.

1.4 Antennas on dielectric substrates

Study of a dielectric lens antenna is related with propagation of electromagnetic waves. Electromagnetic waves are produced by a transmitting antenna. An antenna placed on a semi-infinite dielectric substrate as shown in Figure 1-6 is most sensitive to radiation coming from the dielectric substrate side and tend to radiate most of their power into the dielectric substrate side [27] [28]. The ratio between the radiation power radiated into the dielectric substrate and radiated to the air is $\varepsilon_r^{3/2}$ for an elementary slot antenna and ε_r for an elementary dipole antenna, where ε_r is the relative dielectric constant of the substrate. For instance, Figure 1-7 shows radiation patterns of a printed dipole antenna for different substrates [28]. If the dielectric constant of the substrate increases, more radiation will going to the substrate side. Therefore, in the substrate with high dielectric constant, the radiation pattern can become unidirectional.

(a)   (b)
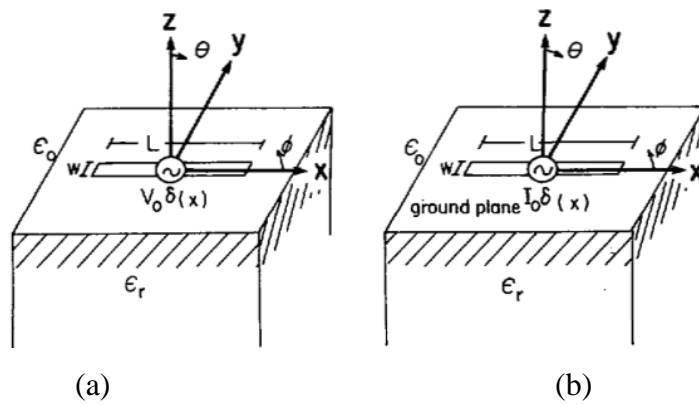
Figure 1-6 Geometry of antennas on a semi-infinte substrate. (a) Printed dipole.
(b) Slot dipole **[28]**.
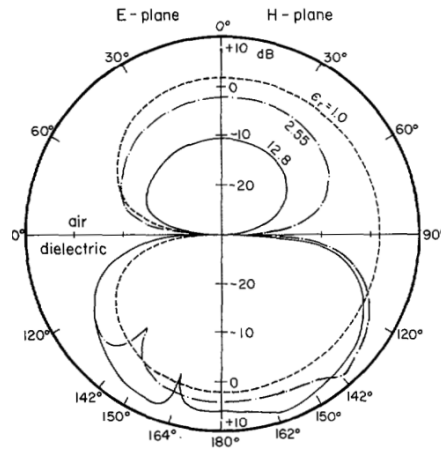
Figure 1-7 Radiation patterns of a printed dipole antenna for different substrates
[28].

For an antenna placed on the dielectric substrate with a finite thickness, from the ray point of view as shown in Figure 1-8, the rays of incident coming from the antenna at angles larger than a critical angle are completely reflected back to the dielectric substrate and trapped in the substrate as surface waves. For example, the critical angle for fused quartz is about 30 degrees. The trapped rays produce surface waves which reduce the radiation efficiency of the antenna. The surface wave should be avoid from the transmitting antenna to obtain good radiation efficiency.

One way to avoid the surface waves is to integrate the antenna on a very thin substrate, typically less than $0.02\lambda_d$ for a dipole antenna and $0.04\lambda_d$ for a slot antenna [29]. We have studied this solution by using electromagnetic simulation (EM) of dipole and slot antenna on substrate at resonant frequency 1 THz [30]. Although the surface waves can be minimized by using the thin substrate, the main issue of this solution is the substrate becomes very thin and fragile at millimeter and sub millimeter-wavelengths in the antenna fabrication process.

11
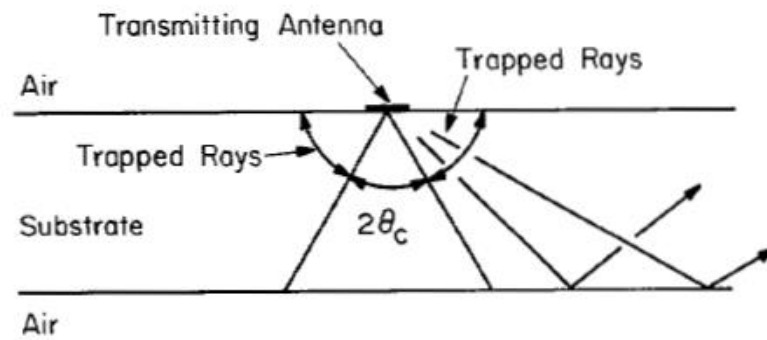
Figure 1-8 A transmitting antenna on a dielectric substrate showing the rays trapped as surface waves. The critical angle $\theta_c = 30^o$, an appropriate for fused quartz ($\varepsilon_r = 4$) [31].

Another attractive method is to place the antenna on the back side of a dielectric lens antenna which has same dielectric constant [32], therefore, the rays are nearly normal to the surface and do not suffer total internal reflection as shown in Figure 1-9. If there is no lens attached to the back of a THz source (a THz antenna), most of the generated radiation remains trapped in the THz source substrate because of the total internal reflection [33]. The structure of the dielectric lens does not support surface waves. The dielectric lens also allows free-space propagation of the THz waves [34]. The use of the dielectric lens antenna takes advantage of the sensitivity of an antenna to radiation coming from the substrate side and eliminates the surface waves.
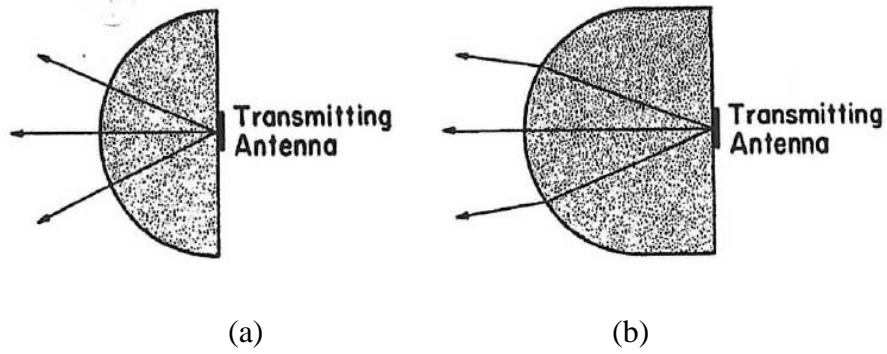
Figure 1-9 Dielectric lenses antenna : (a) hemisphere, (b) extended-hemisphere
[27].

Generally, there are two types of substrate lens as shown in Figure 1-9: hemisphere and extended-hemisphere. Both substrate lenses can be used to avoid the surface waves from the transmitting antenna. The extended hemispherical dielectric lens antenna is an attractive and practical element used in THz systems to focus and collimate beams of the THz wave radiation. By adjusting the extension length to the focal point and placing a detector or an emitter at around the focal point, we can improve coupling efficiency of the THz system. A study of an extended hemispherical dielectric lens antenna with a double-slot antenna feed shows that the directivity, the far-field patterns and the Gaussian-beam coupling efficiencies are strongly dependent on the extension length (especially at high frequencies) [29]. The dielectric lens antenna has been used also for focusing, collimating, expanding and reducing beams of THz wave radiation in quasi-optical systems such as an emitter and a receiver [35]. The dielectric lens antenna also provides compactness as well as mechanical rigidity, thermal stability and a property to eliminate substrate modes of the integrated circuit antenna [36].

1.5 Design a silicon lens antenna for THz application

So far, researches on silicon (Si) lens, as one of the dielectric lens antennas, have been reported by a number of groups [35] [33] [37] [38]. The Si-lens antenna have been used widely to improve coupling efficiency in a THz quantum cascade laser (QCL) [39], a photoconductive antenna (PCA) [40], a hot electron bolometer (HEB) [41] and an antenna coupled detector [42]. A linearly polarized radiation is ordinary in the THz systems. Therefore, it is important for designing THz systems to supply a precise method to evaluate a power-flow-density distribution of polarized THz radiation in the optical systems using the Si-lens antennas.

In the high frequency (optics), the transmission of a spherical or plane wave through an arbitrarily curved dielectric interface can be solved by the geometrical optics theory [43]. By following the Snell's law of refraction, the rays are bent when passing through a boundary between the two different media. In a spherical convex boundary between air and a dielectric material, the rays are converged into a focus. In an optical, a ray-tracing technique is widely used to analyze beam patterns in the optical path [35]. In a quasi-optical system, the ray-tracing method based on the geometrical optics theory is also used to analyze beam of THz wave radiation and the power-flow density distribution by using a number-density of rays. Because linearly polarized radiation is ordinary in the THz systems, a practical method to calculate a precise profile of power-flow density distribution of the polarized THz wave radiation is important to design a silicon lens antenna. The ray-tracing method is, therefore, not enough for evaluating correct radiation-power refracted by a lens, because the incoming rays reaching at different positions on a curved lens-surface have different angles of incidence and different transmittances according to the Fresnel's law of transmission.

Analysis of complex electrically large structures using electromagnetic analysis method, such as the method of moments (MoM), finite element method (FEM), and finite difference time domain (FDTD) method, can become prohibitive due to the need for large computational resources, especially at high frequency,

14

such as in the THz wave region [44]. These methods are complete analysis for electromagnetic problems. These methods are powerfull method applied in microwave or lower frequencies application. On the other hand, asymptotic methods such as geometrical optics (GO) [43] and physical optics [45] require much less computational resources and are effective in modelling electrically large structures but only for far-field calculations at high frequencies. Spectral Domain Ray tracing (SRT) based on spectral theory of diffraction (STD) has been proposed to improve the limitation of the geometrical optics in lower frequencies [44]. The SRT represented the spectral samples of the plane waves as ray tubes that leave the source plane and reach observation point. The geometric theory of diffraction (GTD) is applied to these rays, where they undergo reflections, refractions, and diffractions. The SRT method is shown to be as accurate as FEM and yet computationally fast [44] [46].

In this study, we propose a ray-tracing method combined with Fresnel's transmission to calculate power-flow-density distribution in a silicon lens antenna irradiated with linearly polarized THz wave. We present the distribution of power-transmittance on the spherical boundary of the Si-lens antenna and the power-flow-density distribution inside the Si-lens antenna calculated by our proposed method. Our proposed method is a non-electromagnetic calculation method; therefore, it does not use complex calculations of Maxwell's equation and can be used to avoid large calculations due to the large dimension of the silicon lens antenna relative to the wavelength at the THz region. We compare our results with the calculations by an electromagnetic (EM) and a regular ray-tracing simulator.

1.6 An extended hemispherical silicon lens antenna

An extended hemispherical dielectric lens is a practical element, since the dielectric lens coupled to quasi-optical system is simply adjusted by varying the extension length behind the hemispherical [36]. When the dielectric lens is irradiated with THz wave radiation, the THz wave radiation passing through the

hemisphere boundary is focused inside the dielectric lens antenna. The highest number of power-flow density distribution is existed around the focus in the extension. If a bolometer type detector which detects the radiation power on its surface is placed around the focus in the extension, the detector detects the highest power-flow density. As a result, the detector coupled to the dielectric lens has better detection than without the dielectric lens. If the silicon lens is coupled to an antenna type detector, the extension length can be determined by matching the focusing beam with a main beam of the antenna radiation pattern. In the antenna theory, the coupling is a similar technique as use the dielectric lens antenna for a reflector antenna. Therefore, most energy from the focusing beam can be absorbed by the antenna type detector.

Based on ray-tracing method simulated with an optical ray-tracing software (Zemax), Figure 1-10 shows a parallel rays of incidence travelling from air to a Si-lens antenna. On the hemisphere boundary, the incoming rays are refracted and transmitted into the Si-lens antenna. After passing through the hemisphere boundary, the rays are collected into a focus in the extension of the Si-lens antenna. The changes of the rays' densities indicate the changes of power-flow density distribution. When we calculate the power-flow density distribution inside the Si-lens antenna for linearly polarized THz wave radiation, we should consider the THz wave polarization and transmittances occur at the hemisphere boundary, which is not considered by the ray-tracing method. Polarization is direction of the electromagnetic wave's oscillation. Transmittance is a ratio of the radiation power passed through the hemisphere boundary to the power of incidence. Based on Fresnel's equation of transmission, there are two components of transmittance, i.e. parallel (T_P) and perpendicular (T_S) components. When a ray come from medium 1 (n_1) to medium 2 (n_2) with different refractive index, the two components are determined by the plane of incidence and direction of the THz wave polarization. The angle of incidence and the plane of incidence for a ray passed through the hemisphere boundary is different than other rays, therefore, this condition leads to different transmittances of every ray passing through the hemisphere boundary. Because the transmittance is a ratio of the transmitted power to the power of

incidence, the calculation of the power-flow density distribution inside the Si-lens antenna is not only affected by the density of the rays but also the transmittance depending on the power of incidence, the angle of incidence, the plane of incidence and the rays polarization.
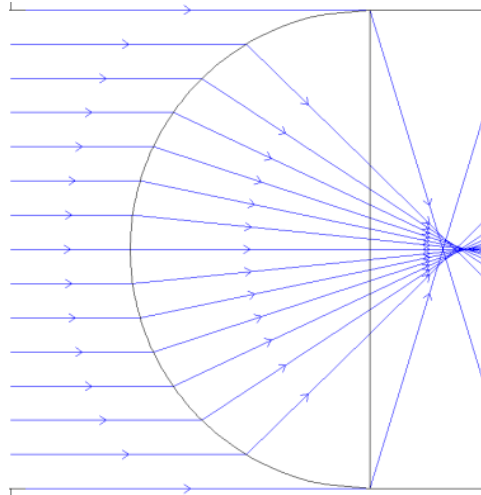
Figure 1-10 Parallel rays travelling from air to a Si-lens antenna simulated with an optical ray-tracing software (Zemax).

1.7 Soda-lime glass for a THz wave attenuator

Among components in a THz system, an attenuator is a component needed to prevent a saturated power when the THz waves detected by a detector. In general, two techniques are used to attenuate power of THz waves: metal grid technique [47] and substrate-based optical elements [48] [49]. The metal grids diffract THz waves and absorb the rejected power. This technique can provide wide band spectrum from 0.7 to 1200 μm [50]. The precision fabrication of the metal grids and effective absorption wall are important points to obtain a precise attenuation. The other technique, which use a substrate with a particular thickness and attenuation level to attenuate the emitted power, is simpler than the metal grids. A set of the substrate attenuators can be arranged to achieve different levels of attenuation [51], [52]. To

be able used in the THz range, a proper material for the substrate attenuator should have low dispersion of refractive index in the THz range. Optical characteristics, such as refractive index, absorption coefficient and attenuation level, are necessary to determine whether a material is appropriate to be used as an attenuator of the THz waves.

In this research, we propose a low cost material of an ordinary glass or also known as soda-lime glass to effectively attenuate power of THz waves. We study attenuation level of the glass at frequency 250 GHz. Three experiments are done to obtain measurement data for the attenuation analysis: THz wave measurement with a pyro detector, THz wave measurement with a body scanner system and refractive index measurement with a transmission THz time domain spectroscopy system (THz-TDS). By using statistical analysis, we analyze the attenuation measured with the pyro detector and then compare with results obtained from the body scanner measurement.

1.8 Purpose of this work

First purpose of this work is to provide a precise method for evaluating power-flow density distribution focused by a Si-lens antenna irradiated with linearly polarized THz wave radiation at frequency one THz. The proposed method combines the ray-tracing method and Fresnel's transmission to include the linearly polarized THz wave parameters. The evaluation of the power-flow density distribution around the focus and the focusing pattern of the transmitted THz wave power are necessary for designing the dielectric lens, which is used to improve the THz wave detectors. In this research, we consider a high-resistivity silicon for the dielectric lens antenna, which has a very low dispersion of refractive index and low absorption in the THz wave range. Therefore, the proposed method is applicable for calculating the power-flow density distribution focused by the silicon lens in the wide range of THz region.

The second purpose in this thesis is to obtain attenuation characteristics of an ordinary glass at the THz wave region. The attenution characteristics are studied by using a 250 GHz THz wave source which radiates the THz waves passing through the glass. Two method are used to detect the THz wave after passing through the glass: a THz pyro detector and a body scanner system. A transmission THz Time-Domain spectroscopy measurement is also conducted to provide refractive index data of the material for the attenuation analysis. The measured signals as a function of the glass thickness are analyzed statistically to extract the attenuation variable. We expect that the glass attenuator as a practical method and also a low cost component to be applied in THz systems. The attenuation characteristics obtained from this study can be utilized to improve performance of THz systems, such as to adjust THz source power irradiated to an object in an active measurement of a THz body scanner system.

1.9 Thesis Outline

This thesis is organized into six chapters.

Chapter 1 gives an overview of research background, materials for THz application, quasi-optical systems, antennas on dielectric substrate, design of silicon lens antenna for THz application, basic principles of an extended hemispherical dielectric lens, purpose of research, soda-lime glass for a THz wave attenuation and outline of this thesis.

Chapter 2 is a review of some basic theories underlying the proposed method. The discussion of geometrical theory as a basis of the ray-tracing method, Snell's law of reflection and refraction, and Fresnel equations are reviewed for bridging the discussion in the next section.

Chapter 3 explains research methodology of the proposed method. Parameters of the Si-lens antenna model, derivation of the mathematical calculation, and the analysis parameters are explained in this chapter.

Chapter 4 is discussing the results of our proposed method and its comparison with other calculation method (EM simulation and regular ray tracing simulation). Transmittance distribution of linearly polarized THz wave radiation on the hemisphere boundary is discussed to understand the effect of the Fresnel's transmission. In the extension of the hemisphere, the discussion is done to understand the power-flow density distribution and the focusing pattern. The power-flow density distribution of linearly polarized THz plane waves irradiated to the Si-lens antenna is calculated by the proposed method and compared with the EM-simulation. The focusing represented with the radius of circles calculated with the proposed method is compared with the pattern calculated with regular ray-tracing method to know the effect of the Fresnel's transmission.

Chapter 5 is discussing experiments and the measurement data analysis to study attenuation characteristics of an ordinary of soda-lime glass at frequency 250 GHz. Three measurements (transmission THz time domain spectroscopy, pyro detector, and body scanner) are conducted to provide the measurement data for the analysis. Statistical analysis method of least-square to an arbitrary and linear function utilized to analyze the attenuation characteristics of the observed glass are discussed in this chapter.

Chapter 6 contains conclusions and provides suggestion of this result to be considered in the future research.

CHAPTER 2
GEOMETRICAL OPTICS AND FRESNEL'S EQUATIONS FOR TRANSMISSION AND REFLECTION

2.1. Geometrical optics

Geometrical optic theory is basic principle of the ray-tracing method. The method is tracing the path of a ray of light through a system by calculating the angle of refraction and the angle of reflection at every surface. In this section, we are discussing three basis laws of geometrical optics, Snell's law and total internal reflection [53].

The three laws as the basis of geometrical optics are the law of rectilinear propagation, the law of reflection, and the law of refraction. The law of rectilinear propagation states that in a homogeneous medium light travels along straight paths. To formulate the laws of reflection and refraction, we consider a ray of light impinging upon a plane surface of separation between two transparent substances, 1 and 2; for example, air and water (Figure 2-1). Assume that each of the two substances is homogeneous and isotropic, the latter qualification meaning that its properties are the same in all directions. We find, in general, that the incident ray splits into two: a reflected ray, which goes back into the medium from which the incident ray came, and a refracted ray that penetrates the other medium. We also find that:

1. The incident ray AO, the reflected ray OA', and the refracted ray OB lie in a plane perpendicular to the boundary surface, called the plane of incidence.
2. The incident ray and the reflected ray form equal angles with the normal NN' to the boundary surface.
3. If θ_1 is the angle between the incident ray and NN' (angle of incidence), and θ_2 is the angle between the refracted ray and NN' (angle of refraction).

The last statement, called Snell's law, has the analytical expression of Equation 2-1. The constant n_{12} is called the index of refraction of the second medium relative to the first medium. The index of refraction of substance 1 relative to substance 2 is the reciprocal of the index of refraction of 2 relative to 1; that is, $n_{12} = 1/n_{21}$. This amounts to saying that if a light ray can follow the path OAB in passing from the first medium to the second, it could also follow the inverse path BOA in passing from the second to the first.

$$\frac{sin\theta_1}{sin\theta_2} = n_{12} \qquad \text{(2-1)}$$
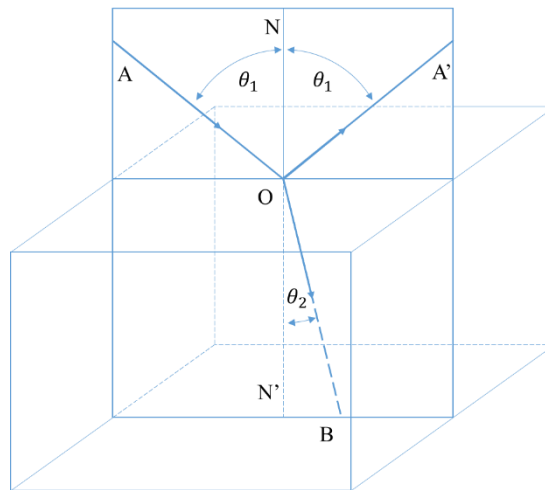
Figure 2-1 Reflection and refraction of a light ray at the boundary between two different transparent media.

Notice that the refraction brings a ray closer to the normal or farther from it depending on whether n_{12} is larger or smaller than one. If $n_{12} < 1$, the angle of refraction becomes equal to $\pi/2$ when $sin \theta_1 = n_{12}$. For such an angle of incidence, the refracted angle goes off at a grazing angle. For a larger angle of incidence, Equation 2-1 cannot be satisfied by any value of θ_2. The refracted ray no longer exists and the light ray is completely reflected back into the medium from which it came. This phenomenon is known as total internal reflection. For example, the

index of refraction of water relative to air is (about) 1.33, and that of air relative to water is (about) 1/1.33. The angle whose sine equals 1/1.33 is 49º. Thus, rays coming from a source under water are totally reflected at the surface of the water if their angles of incidence are greater than 49º.

Total internal reflection in a glass prism is often used to deflect a light through an angle of 90º (Figure 2-2). The cross section of such a prism (called a totally reflecting prism) is a right isosceles triangle. The light ray enters the prism perpendicularly through the face *a*, and strikes the hypotenuse face *b* at an angle of 45º, which is greater than the limiting angle for total reflection for all kind of glass. Total reflection at the hypotenuse surface causes the light ray to emerge from the prism perpendicularly through the face *c*.
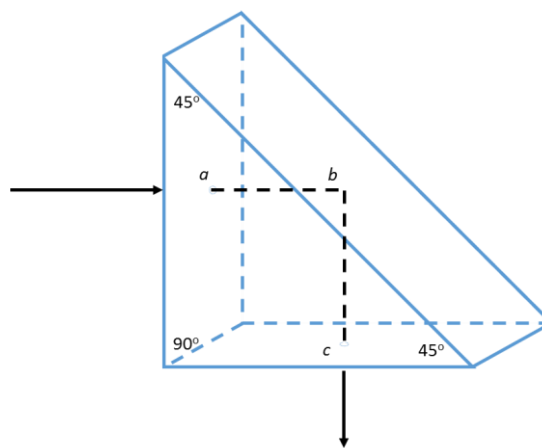
Figure 2-2 Total internal reflection of a ray at the surface of hypotenuse face b in a glass prism.

The index of refraction is usually slightly different for light of different colors, which is known as dispersion. When a ray of white light gives rise, upon refraction, to a fanlike bundle of colored rays as illustrated in Figure 2-3 indicating that the white light results from the superposition of light of different colors. In this study,

we assume that we are researching with single wavelength, so that we may neglect the dispersion.
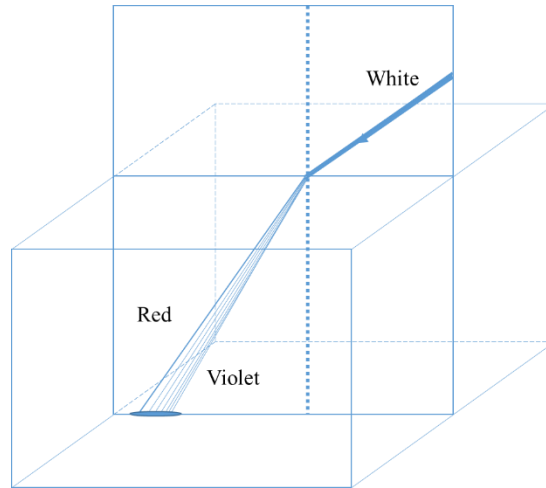
Figure 2-3 Dispersion of a ray of white light

2.2. Fresnel reflection and transmission coefficient

In this section, Fresnel equations are discussed by considering two types of wave polarization vector, which are parallel polarization and perpendicular polarization refer to the plane of incidence [54]. The Fresnel equations of reflection and transmission are discussed to explain the reflection and transmission phenomenon of electric field affected by the wave polarization when propagating between two different medium.

A wave of arbitrary polarization may be described as the superposition of two orthogonally polarized wave, one with its electric field parallel to the plane of incidence (parallel polarization) and the other with its electric field perpendicular to the plane of incidence (perpendicular polarization). These two polarization configurations are shown in Figure 2-4. Polarization with **E** perpendicular to the plane of incidence is also called transverse electric (TE) because E is perpendicular

to the plane of incidence, and that with E parallel to the plane of incidence is called transverse magnetic (TM) because the magnetic field that is perpendicular to the plane of incidence.

(a)

(b)
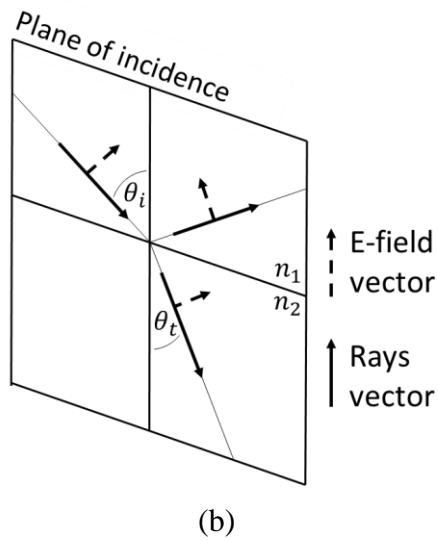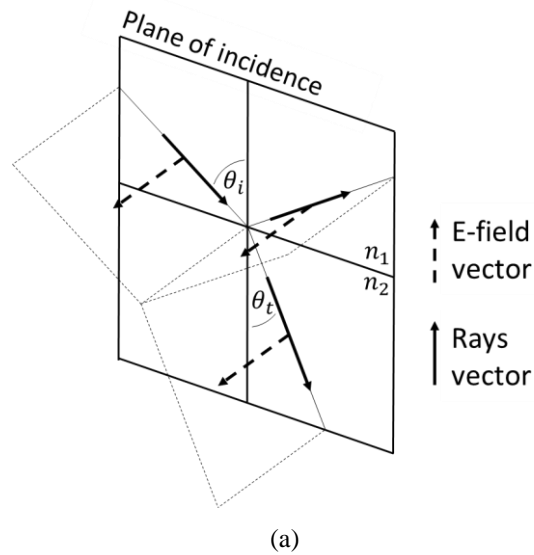
Figure 2-4 Schematic of a plane of incidence, a ray of incidence, a ray of reflection, a ray of transmission, and the polarization vector for polarization (a) perpendicular and (b) parallel to the plane of incidence.

Figure 2-4 (a) shows perpendicularly polarized incident plane wave propagation come to a boundary between medium 1 and medium 2. Equations 2-2 and 2-3 are expressions for the Fresnel reflection and transmission coefficients in the perpendicular case, respectively. These two coefficients are formally known as the Fresnel reflection and transmission coefficients for perpendicular polarization. The two coefficients are related by Equation 2-4. If medium 2 is a perfect conductor $(n_2 = 0)$, Equation 2-2 and 2-3 reduce to $r_s = -1$ and $t_s = 0$, respectively, which means that the incident wave is totally reflected by the conducting medium or there are no waves transmitted into the medium 2.

$$r_s = \frac{E^r{}_s}{E^i{}_{s0}} = \frac{n_1 \cos\theta_i - n_2 \cos\theta_t}{n_1 \cos\theta_i + n_2 \cos\theta_t} \qquad (2\text{-}2)$$

$$t_s = \frac{E^t{}_s}{E^i{}_{s0}} = \frac{2n_1 \cos\theta_i}{n_1 \cos\theta_i + n_2 \cos\theta_t} \qquad (2\text{-}3)$$

$$t_s = 1 + r_s \qquad (2\text{-}4)$$

Figure 2-4 (b) shows parallel polarized incident plane wave propagation come to a boundary between medium 1 and medium 2. Equations 2-5 and 2-6 are expressions for the Fresnel reflection and transmission coefficient for parallel polarization, respectively. The two coefficients are related by Equation 2-7. When the second medium is a perfect conductor with $n_2 = 0$, the incident wave gets totally reflected at the boundary. This condition is same for both the parallel polarization and the perpendicular polarization, which gives $r_p = -1$ and $t_\perp = 0$ meaning that the incident wave is totally reflected by the conducting medium or there are no waves transmitted into the medium 2.

$$r_p = \frac{E^r{}_p}{E^i{}_{p0}} = \frac{n_1 \cos\theta_t - n_2 \cos\theta_i}{n_1 \cos\theta_t + n_2 \cos\theta_i} \qquad (2\text{-}5)$$

$$t_p = \frac{E^t{}_p}{E^i{}_{p0}} = \frac{2n_1 \cos\theta_i}{n_1 \cos\theta_t + n_2 \cos\theta_i} \qquad (2\text{-}6)$$

$$t_p = \left(1 + \mathbf{r}_p\right)\frac{\cos \theta_i}{\cos \theta_t} \qquad\qquad (2\text{-}7)$$

Figure 2-5 shows Fresnel reflection and transmission coefficient as a function of the angles of incidence of waves moving from air to water with refractive index 1.33. Figure 2-5 (a) shows the transmission coefficient decreases of the angles of incidence increases. On the other parameter, absolute of the reflection coefficient shows that the transmission coefficient increases if the angles of incidence increases. In the case of the parallel polarization, Figure 2-5 (b) shows a Brewster angle condition, which is defined as the angle of incidence at which the Fresnel reflection coefficient equal zero, is occur at about 53 degrees. At the Brewster angle, the parallel-polarized component of the incident wave is totally transmitted into medium 2. The Brewster angle is also called the polarizing angle. This is because, if a wave composed of both perpendicular and parallel polarization components, the parallel polarized component is totally transmitted into the second medium, and only the perpendicularly polarized component is reflected by the surface.

These coefficients are fractional amplitudes, and must be squared to get intensities for reflection and transmission. But, the square of the transmission coefficient gives the transmitted energy flux per unit area (intensity), and the area of the transmitted beam is smaller in the refracted beam than in the incident beam if the refraction is less than that of the incident medium. When we take the intensity times the area for both the reflected and refracted beams, the total energy flux must equal that in the incident beam [55].
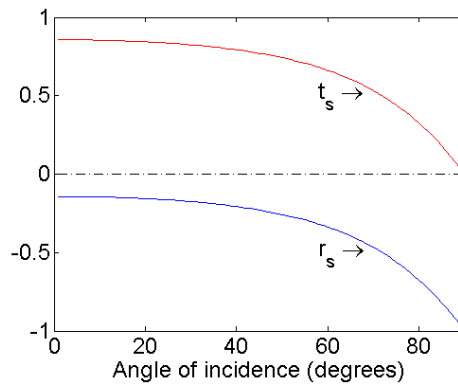
(a)
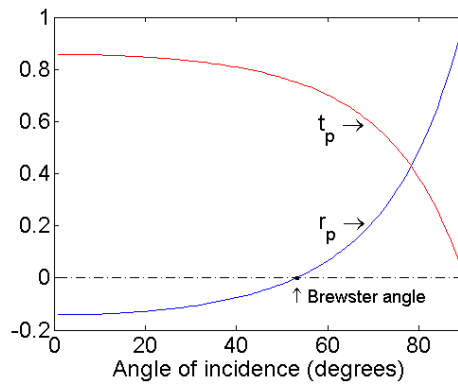
(b)

Figure 2-5 Plot for Fresnel reflection and transmission coefficient, which is calculated from air to water (*n*=1.33), for (a) perpendicular polarization and (b) parallel polarization.

2.3. Reflectance and transmittance

The reflectivity (also called reflectance in optics) is defined as the ratio of the reflected power to the incident power. Power of the polarized wave is proportional to the square of its amplitude. Therefore, the reflectance for perpendicular polarization and parallel polarization are defined as the square of the Fresnel reflection coefficient defined by Equations 2-8 and 2-9, respectively.

$$R_s = |r_s|^2 \qquad \text{(2-8)}$$

$$R_p = |r_p|^2 \qquad \text{(2-9)}$$

The transmittivity (or transmittance in optics) is defined as the ratio of the transmitted power to incident power. The incident, reflected, and transmitted waves have to obey the law of conservation energy. Conservation of the power requires that the incident power equals the sum of the reflected and transmitted powers. Therefore, the transmittances for perpendicular polarization and parallel polarization are defined by Equations 2-10 and 2-11, respectively. Figure 2-5 shows the reflectance and the transmittance of waves from air to water with refractive index 1.33. The maximum transmittance of the perpendicular polarization as shown in the Figure 2-5 (a) is at the zero degrees, then, the transmittance decreseas as the angle of incidence increase. Figure 2-5 (b) shows the transmittance increases from zero degree to the Brewster's angle, then, it decreases afterwards. Because at the Brewster's angle can transmit almost perfectly one transmittance component of non-polarized radiation, the reflected wave become polarized radiation. This phenomenon is often utilized to polarize the electromagnetic radiation.

$$T_s = 1 - R_s \qquad \text{(2-10)}$$

$$T_p = 1 - R_p \qquad \text{(2-11)}$$
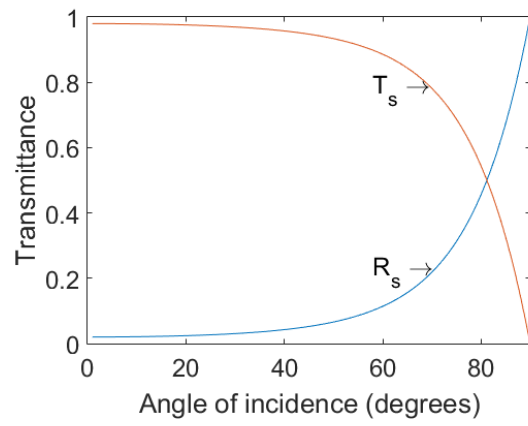
(a)
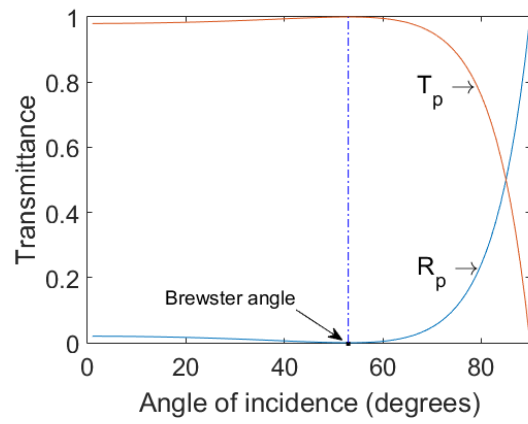
(b)

Figure 2-6 Plot for Fresnel reflectance and transmittance, which is calculated from air to water (n=1.33), for (a) perpendicular polarization and (b) parallel polarization.

CHAPTER 3
METHODHOLOGY TO CALCULATE THE RADIATION-POWER-FLOW DISTRIBUTION IN A SILICON LENS ANTENNA IRRADIATED WITH LINEARLY POLARIZED RADIATION

3.1 Model of a Si-lens antenna

A schematic of an extended hemispherical Si-lens antenna irradiated by a parallel beam of THz wave and incoming, reflected and refracted (transmitted) rays are shown in Figure 3-1 (a) and (b), respectively. Direction of the ray of incidence is same as the z-axis direction. The Si-lens antenna consists of two parts: a hemisphere and an extended cylinder. In this study, the radii (R) of the hemisphere and the extension length (d) are set to 2 mm and 1 mm, respectively. The sizes are considered as an appropriate dimension to couple the incoming radiation at frequency around 1 THz. The material of the lens antenna is high-resistivity silicon (dielectric constant, ε_r = 11.7 at 1 THz), which has a very low dispersion of refractive index and low absorption in the THz wave range [24].

We consider the silicon lens antenna is irradiated with plane waves. The plane waves is as an approach of far-field radiation from a transmitting antenna. The wave front of the plane waves are planes, therefore, the plane wave wavefronts is represented by a parallel rays of incidence.
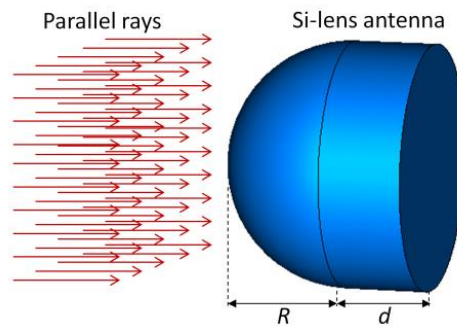
(a)
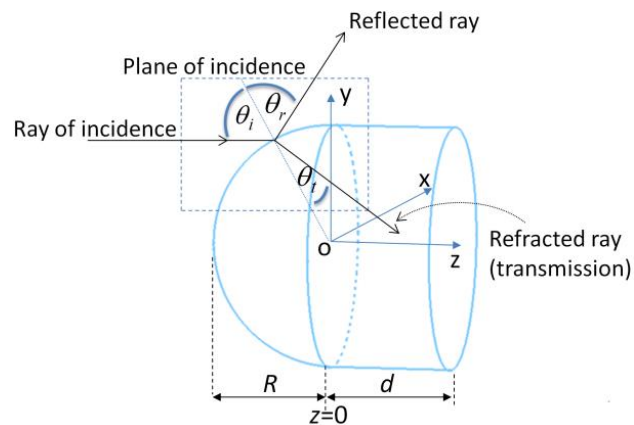
(b)

Figure 3-1 (a) Illustration of a model of a Si-lens antenna and parallel rays of incoming radiation. (b) Schematic of incoming, reflected and transmitted (refracted) rays around the boundary of air to a Si-lens antenna. R and d are a radius of a hemisphere and a length of extension of the hyper hemispherical lens, respectively.

When the parallel rays traveling to the z-direction reach the Si-lens antenna between air and the hemisphere boundary of the Si-lens antenna, some radiation power is reflected back to air and the rest is transmitted and refracted. When the rays of incidence reach the hemisphere boundary, three kinds of angles are formed as shown in Figure 3-1 (b). The angle of θ_i, θ_r and θ_t are the angle of incidence, the angle of reflection and the angle of refraction, respectively. The three angles are determined from the normal vector. The normal vector (dashed line) is obtained by

making a line from the center of the hemisphere to the observed hemisphere boundary where the rays of incidence hit the hemisphere boundary. For every ray of incidence, the normal vector, and the ray of refraction (transmission), a plane of incidence is shown in Figure 3-1 (b) as a rectangular dashed line. In a plane of incidence, we find that the radius length of the hemisphere is a hypotenuse of a triangle and the side length in front of the angle of incidence (θ_i) is square root of the coordinate of the observed ray on x-y plane. Therefore, we can use Equation 3-1 to calculate the angles of incidence (θ_i) for the rays of incidence that reach the hemispherical boundary. Based on Snell's law of refraction as defined in Equation 3-2, the angles of refraction (θ_t) are calculated by considering the refractive index of air or medium 1 $(n_1 = 1)$ and the refractive index of the Si-lens material $(n_2 = \sqrt{\varepsilon_r})$. Because refractive index of the medium 2 is higher than the medium 1, the angles of refraction (θ_t) are smaller than the angles of incidence. Therefore, the transmitted rays seem to be bent after passing through the hemisphere boundary and collected at around a focus in the extended length. At the boundary, we also calculate the two component of Fresnel's transmission depending on the irradiated waves' polarization. After passing through the hemisphere boundary, the transmitted rays are traced in the Si-lens antenna.

$$\theta_i = sin^{-1}\left(\frac{\sqrt{x^2+y^2}}{R}\right) \qquad\qquad (3\text{-}1)$$

$$\theta_t = sin^{-1}\left(\frac{n_1}{n_2}sin(\theta_i)\right) \qquad\qquad (3\text{-}2)$$

3.2 Method to calculate the power-flow density distribution focused by a Si-lens antenna

Based on Fresnel's law of transmission as defined in Equations 3-3 and 3-4, we calculate transmittances for all transmitted rays when pass through the hemisphere boundary by taking into account the angles of incidence (θ_i), the

refractive indices of air and silicon (n_1, n_2), the angles of refraction (θ_t), the planes of incidence, and the THz wave polarization. Two transmittance components (T_P and T_S) are calculated depending on the THz wave polarization. Wave polarization is vectors of electric field (E-field) oscillation, which can be divided into two components, refer to the plane of incidence: the parallel component $\left(\overrightarrow{E_P}\right)$ and the perpendicular component $\left(\overrightarrow{E_S}\right)$. Figure 3-2 shows the vector of the THz wave polarization and the plane of incidence (dash line) determine vector of the two transmittance components of the transmitted rays. In this study, we consider the direction of the THz wave polarization is parallel to the x-axis (linear horizontal polarization). The parallel component is the component whose vector is parallel to the plane of incidence. The perpendicular component is the component whose vector is perpendicular to the plane of incidence. After the two components are calculated with Equations 3-3 and 3-4, the transmittances of the transmitted rays are deduced with Equation 3-5. Angle of θ calculated by Equation 3-6 is a tangent function from the observed ray on x-y plane.
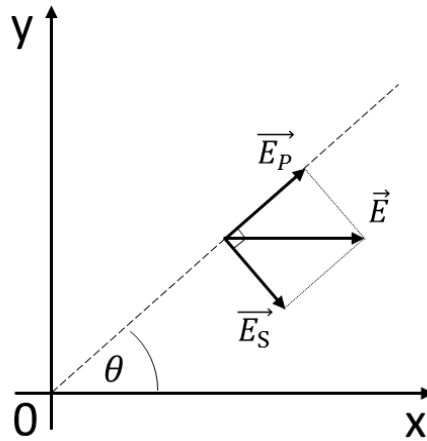
Figure 3-2 E-field vector ($\vec{E}$) of an incoming ray on the x-y plane and the two transmittance components of parallel ($\overrightarrow{E_P}$) and perpendicular ($\overrightarrow{E_S}$) to the plane of incidence around the hemisphere boundary.

$$T_P = 1 - \left| \frac{n_1 \cos\theta_t - n_2 \cos\theta_i}{n_1 \cos\theta_t + n_2 \cos\theta_i} \right|^2 \qquad (3\text{-}3)$$

$$T_S = 1 - \left| \frac{n_1 \cos\theta_i - n_2 \cos\theta_t}{n_1 \cos\theta_i + n_2 \cos\theta_t} \right|^2 \qquad (3\text{-}4)$$

$$T = T_P \cos(\theta)^2 + T_S \sin(\theta)^2 \qquad (3\text{-}5)$$

$$\theta = \tan^{-1}\left(\frac{y}{x}\right) \qquad (3\text{-}6)$$

After direction and transmittances of the rays passed through the hemisphere boundary were identified, we trace the transmitted rays travelling inside the Si-lens antenna. For a transmitted ray travelling from the hemisphere boundary (point C) to z-axis (point A) as shown in Figure 3-3, it makes a triangle of ABC. The angle at point A (θ_A) made by the z-axis and the path of the transmitted rays can be calculated with Equation 3-7 as a function of the angle of incidence (θ_i) and the angle of refraction (θ_t). By considering the triangle OBC and the length of OC equal to the hemisphere radius of the Si-lens antenna, the length of BC can be calculated by Equation 3-8. After the angle at point A (θ_A) and the length of BC have been calculated with Equations 3-7 and 3-8, respectively, Equations 3-9 is used to calculate the length of AB. By using Equation 3-10, we calculate the length of OA to get the distance from the hemisphere center or the origin of the Cartesian coordinates to point A. Equation 3-11 is used to calculate the distance of the transmitted rays from the z-axis. After obtaining the length of y' from Equation 3-11 and the angle of θ from Equation 3-6 for all transmitted rays, we can identify the position of the transmitted rays on x-y planes at a certain position of the z-axis in a format of a polar coordinates ($y' \angle \theta$).

$$\theta_A = \theta_i - \theta_t \qquad (3\text{-}7)$$

$$BC = R\sin(\theta_i) \qquad (3\text{-}8)$$

$$AB = \frac{BC}{tan(\theta_A)} \qquad\qquad \text{(3-9)}$$

$$OA = \left(R - Rcos(\theta_i)\right) + \left(\frac{AB}{tan(\theta_A)}\right) \quad \text{(3-10)}$$

$$y' = (OA - Z_m)tan(\theta_A) \qquad\qquad \text{(3-11)}$$
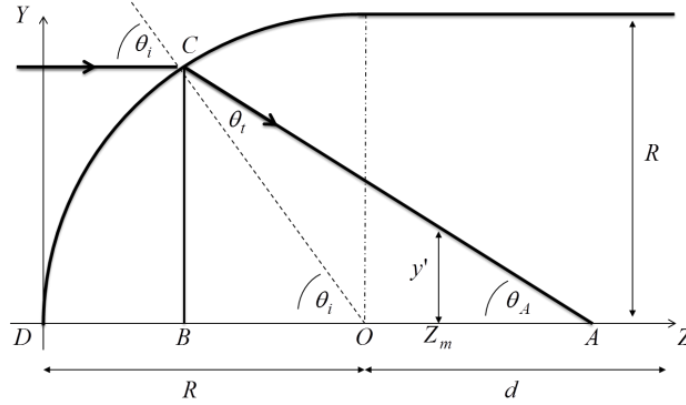
Figure 3-3 Schematic of a ray of incidence and a ray of transmission around the boundary of air to the Si-lens antenna.

Power-flow density distribution for a transmitted ray on planes perpendicular to the z-axis are calculated by taking into account the Fresnel's transmission, and the value of power-flow density in a unit area (VA/m^2) of a ray of incidence. In this study, we determine 1 VA/m^2 as the power-flow density of the rays of incidence (P_I). The power-flow density of a transmitted ray (P_T) is calculated with Equation 3-12 as the power-flow density of a ray of incidence (P_I) multiplied by the Fresnel's transmission (T). Power of the transmitted rays can be calculated by multiplying the power-flow density and the unit area represented by the the transmitted rays.

$$P_T = P_I T \qquad\qquad \text{(3-12)}$$
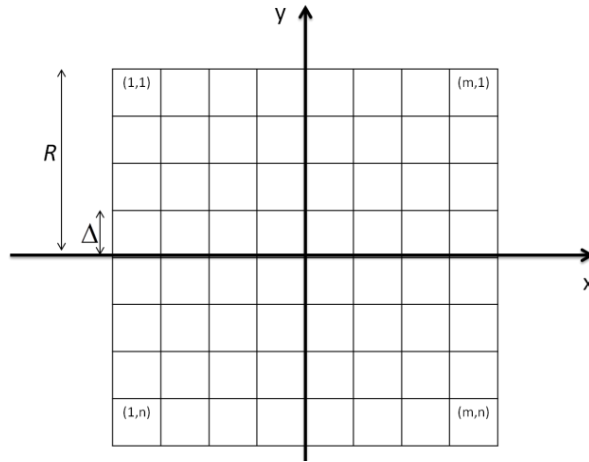
Figure 3-4 Square meshes used to calculate the power-flow density distribution
on the x-y plane.

After all transmitted ray distribution on x-y planes in the Si-lens antenna
have been calculated with Equation 3-6 and 3-11 and the power-flow density of the
transmitted rays calculated with Equation 3-12, then, we calculate power-flow
density distribution on the x-y planes in the extended length. Figure 3-4 shows
square meshes used to calculate the power-flow density distribution. Because the
power-flow density calculation done on the x-y plane, two-dimensional matrix (m,
n) is used to identify the distribution of the power-flow density. For every square
unit has length of delta (ΔR), the power-flow density of every unit area is calculated
by summing the power for all transmitted rays which are located in the same unit
area as illustrated in Figure 3-5. The power density at a particular location of (m, n)
is obtained by dividing the total power with the unit area as described in Equation
3-13.

$$Power - flow\ density = \frac{\sum_{i=1}^{n} P_i}{\Delta R^2}\ [W/m^2] \qquad (3-13)$$

37
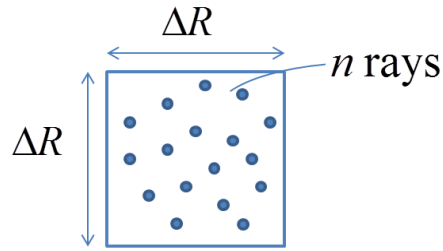
Figure 3-5 Illustration of *n* rays located at a particular unit area with size *ΔR x ΔR*.

Analysis of the power-flow density focused by the Si-lens antenna is done by observing the power-flow density distribution of several x-y planes from the center (z-axis) to the edge of the Si-lens antenna. After the incoming rays passed through the hemisphere boundary, the power-flow density beams on the x-y plane are formed in circles. The radii of the circles are used to find differences of the power-flow density among the observed planes. The radii of circles as a function of the z-axis (z > 0) will show the focusing pattern in the cylinder extension of the Si-lens antenna. We calculate the radii for some different percentages of the total transmitted power in the Si-lens antenna calculated from the center of the circles (z-axis) to the edge of the Si-lens antenna to show the effect of the Fresnel's transmission. The radii for the different percentages are also used to show the concentration of the power-flow density distribution. Figure 3-6 is a flow chart as a summary of the steps of the proposed method.

```
                    ┌─────────────┐
                    │    Start    │
                    └─────────────┘
                           │
                           ▼
                   ╱─────────────╲
                  ╱  Determine    ╱
                 ╱   the initial ╱
                ╱   parameters  ╱
               ╱───────────────╱
                           │
                           ▼
                  ┌──────────────┐
                  │ Rays of      │
                  │ incidence    │
                  │ travelling to│
                  │ the Si-lens  │
                  │ antenna      │
                  └──────────────┘
                           │
                           ▼
                  ┌──────────────┐
                  │ Filter the   │
                  │ transmitted  │
                  │ rays         │
                  └──────────────┘
                           │
                           ▼
                  ┌──────────────┐
                  │ Calculate    │
                  │ variables at │
                  │ the          │
                  │ boundaries   │
                  └──────────────┘
                           │
                           ▼
                  ┌──────────────┐
                  │ Trace the    │
                  │ transmitted  │
                  │ rays         │
                  └──────────────┘
                           │
                           ▼
                  ┌──────────────┐
                  │ Calculate the│
                  │ power-flow   │
                  │ density      │
                  └──────────────┘
                           │
                           ▼
                  ┌──────────────┐
                  │ Calculate the│
                  │ radii of     │
                  │ circles      │
                  └──────────────┘
                           │
                           ▼
                    ┌─────────────┐
                    │   Finish    │
                    └─────────────┘
```
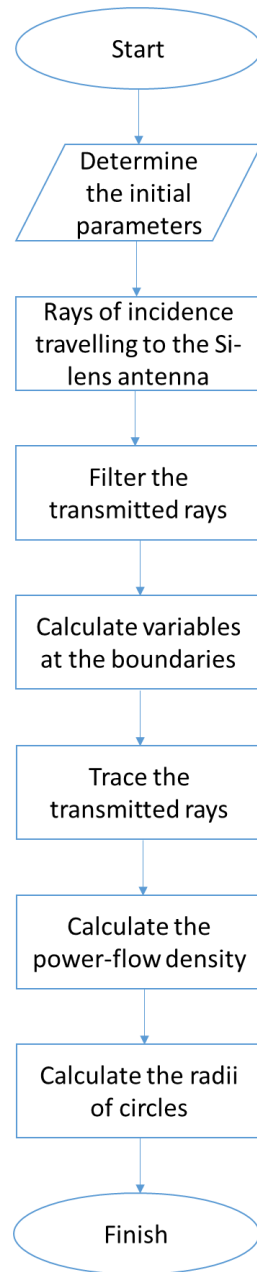
Figure 3-6 Flow-chart of the proposed method to calculate the power-flow density distribution and the radii of circles in the Si-lens antenna

In this study, we carry out the ray-tracing including the Fresnel's transmittance for the incoming rays with a linear polarization parallel to x-axis. We deduce x and y components of transmittance from T_P and T_S for each incoming ray and then x and y components of a transmitted power-flow traveling along each

refracted ray. We derive a transmitted power-flow densities passing through x-y planes to the z-direction for the two components of polarization.

To compare with and confirm the results of the proposed method, we are conducting electromagnetic (EM) simulation with a commercial software of CST Microwave studio 2014. Under the same parameters considered in the proposed method, the power-flow density distribution is simulated by radiating THz plane waves into the Si-lens antenna as illustrated in Figure 3-7. We execute the EM simulation by CST Microwave (MW) studio at several frequencies at the THz range (0.1 THZ to 1 THz) frequencies for the incoming radiation with a linear polarization to see the diffraction effect. We also compare the radii of circles between calculated with the proposed method and simulated with a regular ray-tracing of an optical simulator of Zemax to clarify the difference between them.
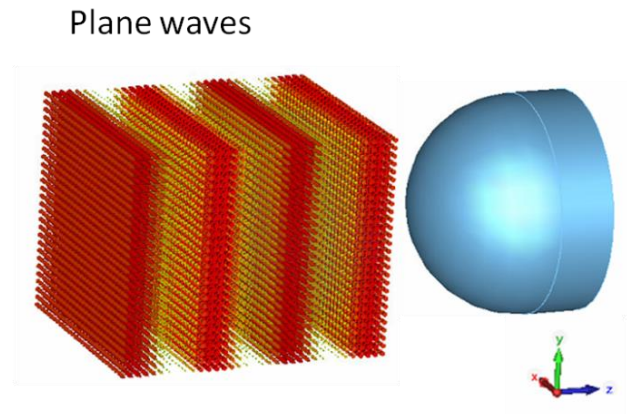
Figure 3-7 An illustration of linearly polarized plane waves irradiated to the silicon lens.

CHAPTER 4

RESULTS AND DISCUSSION OF POWER FLOW DENSITY IN A SILICON LENS IRRADIATED LINEARLY POLARIZED THZ WAVE

4.1 Transmittance distribution

Before we execute calculation by the proposed method and simulation by the EM-simulator and the regular ray tracing simulator, we determined simulation conditions of the Si-lens antenna and the polarized radiation for calculation conducted by the proposed method. Radius of the hemisphere and length of the extended hemisphere are 2 mm and 1 mm, respectively. Those sizes is considered as an appropriate size to be implemented at frequency 1 THz. The dielectric constant (ε_r) of the silicon material is 11.7. Number of data in the proposed method calculation is 256 x 256, therefore, the dimension of the unit area is 0.015625 mm x 0.015625 mm. The THz waves irradiated to the Si-lens antenna have linear (horizontal) polarization, which is parallel to the x-axis. The electric field (rms) of the irradiated THz waves is 1 V/m. From the defined electric field, power flow of the incoming parallel rays in vacuum estimated by considering vacuum permitivity ($\varepsilon_0 = 8.85 \times 10^{-12}$ F/m) and speed of light in free space ($c_0 = 3 \times 10^8$ m/s) is 2.7 x 10^{-3} Watt/m^2. By multiplying the power-flow density with a circular area limited by the hemisphere boundary, the energy coming to the silicon lens is also able to be estimated around 3.39 x 10^{-8} Watt.

Transmittance in power on a spherical boundary of air to the Si-lens antenna is calculated for the parallel incoming-rays with linear polarization using the proposed method. The transmittance shows the ratio between the power transmitted into the Si-lens antenna and the power coming to the Si-lens antenna. Figure 4-1 (a) is the transmittance distribution for the incoming rays with polarization parallel to x-axis, which clearly shows an asymmetrical features. The asymmetrical distribution is due to Fresnel's transmission depending on the angles of incidence and the angles

between the plane of incidence and the polarization-direction of the incoming rays, which varied according to positions on the spherical boundary surface of the Si-lens antenna. To obtain more clearly the different profiles of transmittances on position between the parallel and the perpendicular of the incoming wave polarization, Figure 4-2 (a) and (b) show transmittance on the x-axis (y=0) and y-axis (x=0), respectively, when the linearly polarized THz wave radiation pass through the hemisphere boundary of the Si-lens antenna. On the line y=0, the transmittance becomes purely T_P and the maximum transmittance appears near the edge of the Si-lens because of the zero reflectance (i.e. 100% transmittance) at the Brewster's angle (76.9 degrees) which is close to the edge. On the line x=0, the transmittance becomes purely T_S and the maximum transmittance appears at the center because the reflectance increases and the transmittance decreases monotonously to the edge. The power transmittance estimated by the proposed method is 68.3% of the input radiation power; therefore the estimated transmitted power is 2.2775 x 10^{-08} Watt. The rest of the input radiation power is reflected back to the air.

The incoming rays except for on the lines of x=0 and y=0 have the difference in T_P and T_S referred to the plane of incidence defined by a plane composed of z-axis and the position of incidence, which produces a small component perpendicular to the polarization of incoming rays. We, therefore, display the ratios calculated from the parallel and perpendicular components of the transmitted power referred to the incoming power with a linear polarization in Figure 4-1 (b) and (c), respectively.
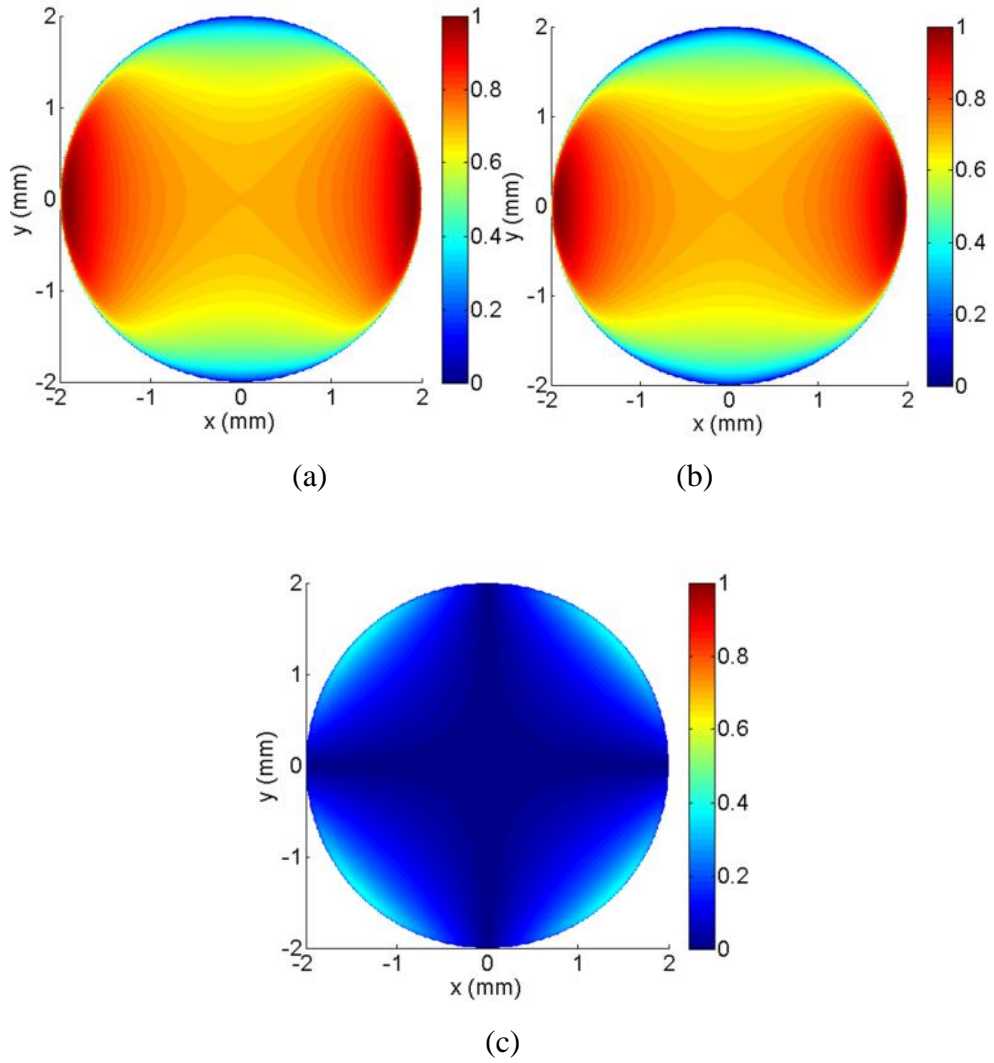
Figure 4-1 Transmittance distributions of THz radiation just after passing from air to the Si-lens for the rays of incidence with linear polarization parallel to x-axis. (a) Transmittance calculated from the total transmitted-power referred to the incoming power, (b) the ratio calculated from the parallel component of the transmitted power to the incoming power, and (c) the ratio of the perpendicular component of the transmitted power to the incoming power.
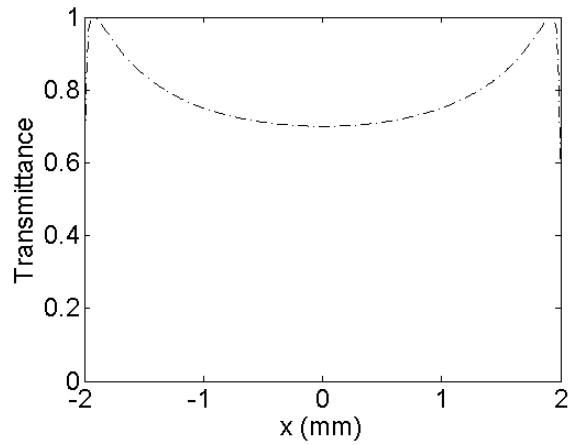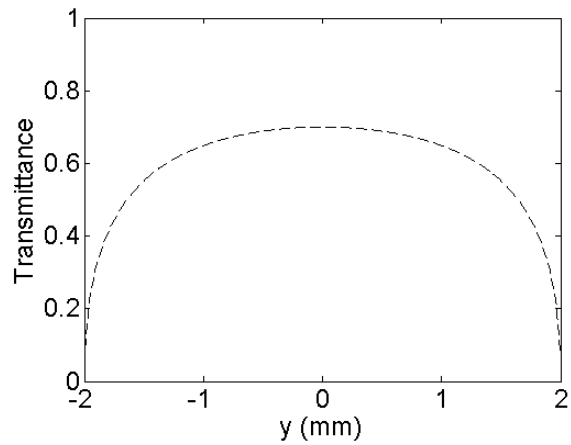
Figure 4-2 Transmittances around the hemisphere boundary from air to the Si-lens antenna on (a) the x-axis and (b) the y-axis.

4.2 Power flow density distribution for frequencies 100 – 700 GHz

In this section, power-flow density distribution comparison between the proposed method and the EM-simulation is conducted for frequencies 100 – 700 GHz of the plane waves irradiated to the Si-lens. Under the same condition, the power-flow density distribution located between the backside plane of the hemisphere and the extended length (at plane orthogonal to the z-axis at z=0 mm)

is calculated by the proposed method and simulated by the EM-simulation. The different frequencies conducted by the EM-simulation is to see effect of diffraction for those frequencies.

Figure 4-3 shows the power flow density distribution at a plane perpendicular to z-axis at z=0 mm calculated with the proposed method. The power-flow density distribution is not a circular pattern but ellipse. The power density-profile at the y=0 mm is wider than the power density profile at the x=0 mm. This result can be explained as the transmittance distribution in the previous section when the Brewster's angle occur if the incoming radiation polarization is linear (horizontal) polarization or parallel to the x-axis. The power flow density around the center (more than 0.02 Watt/m^2) is much higher than power density of the incoming radiation (around 2.7 x 10^{-3} Watt/m^2).
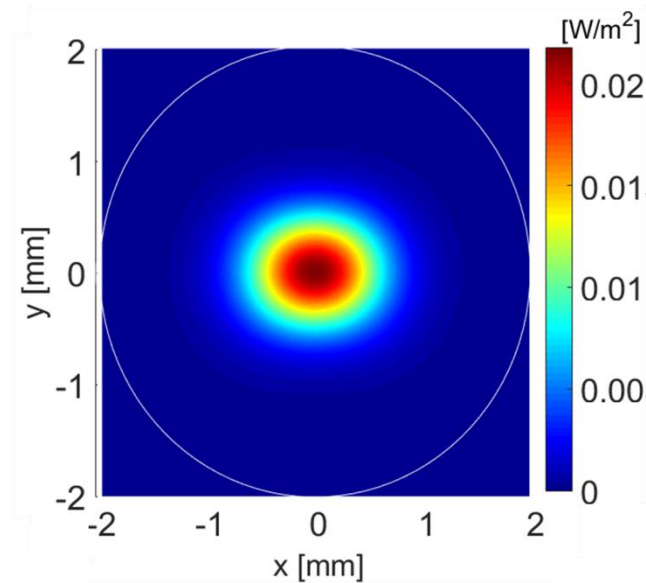
Figure 4-3 Power flow density distribution at the plane orthogonal to z-axis at z=0 mm calculated with the proposed method.

We execute simulation of the power-flow-density distribution for the polarized rays of incidence by the EM-simulation in order to compare the result of the proposed method. Linearly (horizontal) polarized THz plane waves are irradiated to the Si-lens antenna. The electric field (rms) of the irradiated THz waves is 1 V/m. We applied perfectly matched layer boundary on the z-axis to perfectly absorb the plane waves after passing the extended length and to avoid reflection of the plane waves. On the x-axis and y-axis, we applied periodic boundaries to obtain perfect plane waves. The distance between the Si-lens antenna and the periodic boundary is set large to avoid the disturbances of the waves reflected from the adjacent element of the periodic condition.

Figure 4-4 shows the power-density profile simulated by the EM-simulation at Frequency 700 GHz at plane orthogonal to z-axis at z=0 mm. The power flow density distribution is ellipse as obtained by the proposed method (Figure 4-3). The result shows that the linearly polarized radiation produces ellipsoidal beam patterns, which are the effect of the Fresnel's transmission and the circular symmetry irradiation parallel to the z-axis of the Si-lens. From this result, we calculate the energy in the circle, which is 3.3376×10^{-8} Watt. The expected energy following the law of conservation energy is 2.2775×10^{-8} Watt. Therefore, correction factor is necessary to the EM-simulation data for comparison with the proposed method results.
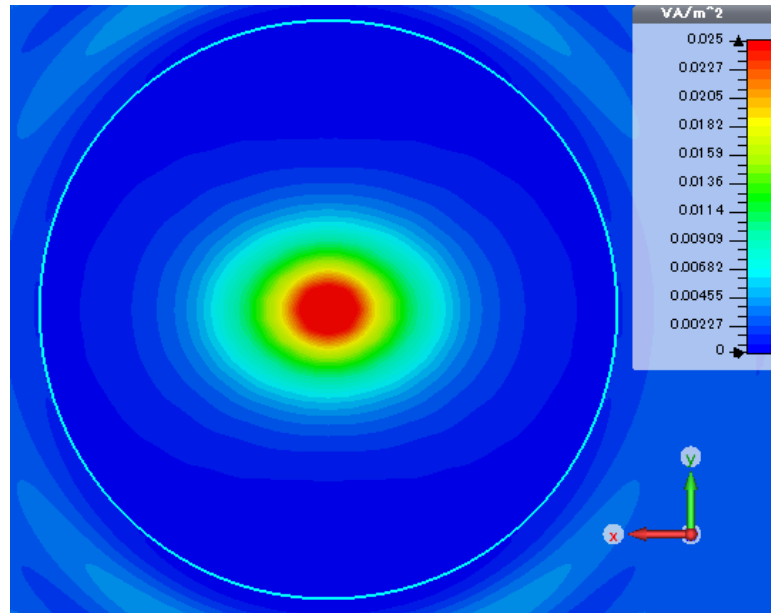
Figure 4-4 Power-flow density distribution simulated by the EM-simulation at frequency 700 GHz at plane orthogonal to the z-axis at z=0 mm.

The energy transmitted into the silicon lens antenna simulated by the EM-simulation of frequency from 100 GHz to 700 GHz is shown in the Figure 4-5. The EM-simulation results shows the transmitted energy, which shift to the law of energy conservation. The discrepancies are affected by diffraction when the wavelength become more comparable to size of the Si-lens. Other factor is three dimensional environment simulation performed by the EM-simulation representing complex conditions which some factor not included in the proposed method. As shown in Figure 4-5, the difference between two method decreases as the frequency increases or the wavelength decreases.
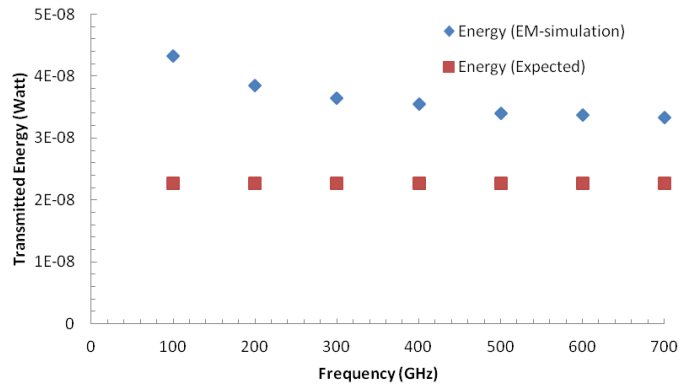
Figure 4-5 Transmitted energy simulated for frequencies 100 – 700 GHz by the
EM-simulation

Figure 4-6 shows the power-flow distribution obtained with the EM-simulation
after applying the correction factor. The ellipsoidal beam patterns is effected by the
Fresnel's transmission and the circular symmetry irradiation parallel to the z-axis
of the silicon lens. Compared to the proposed method in Figure 4-3, the power-flow
at the center, from the proposed method looks higher than the EM-simulation. At
close to the edge, the power-flow from the proposed method is lower than the EM-
simulation. The two results show that the irradiation of 700 GHz linearly polarized
plane waves suffer diffraction which widen the power flow density distribution.
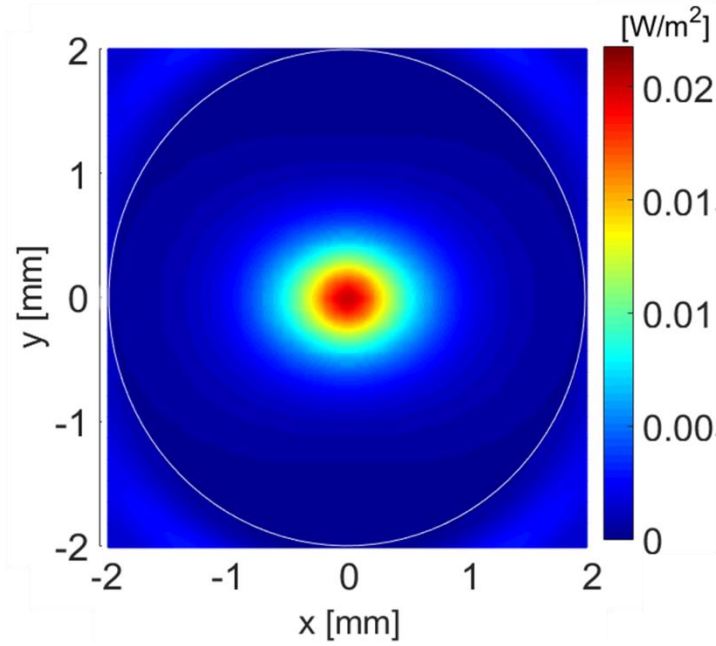
Figure 4-6 Power-flow density distribution simulated by the EM-simulation at frequency 700 GHz at plane orthogonal to the z-axis at z=0 mm.

In order to see more clearly the diffraction effect for the 700 GHz simulation, Figure 4-7 (a) and (b) show the profiles of the power-flow density distribution on 1-dimension at y=0 mm and x=0 mm, respectively. The results simulated by the EM-simulation show the wider power-flow profiles and the lower peak value than the proposed method results.
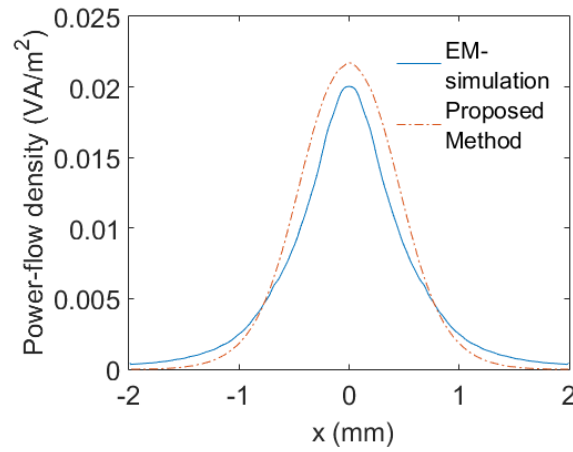
(a)
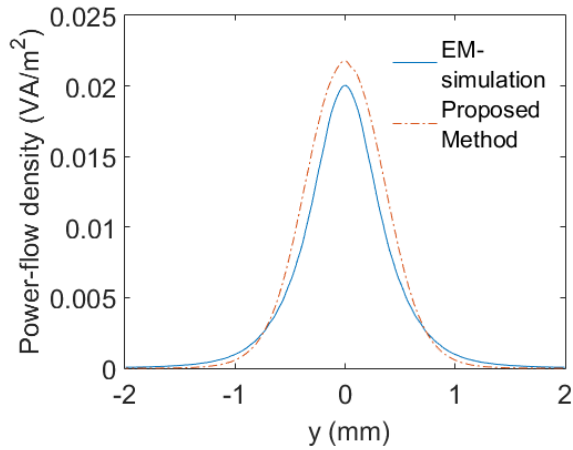
(b)

Figure 4-7 Profiles comparison of the power-flow density distribution at plane z=0 mm between the proposed method and the EM-simulation simulated at frequency 700 GHz. (a) at line y=0 mm and (b) at line x=0 mm.

The effect of the diffraction occur in the Si-lens simulation can be seen in the EM-simulation for different frequencies as shown in Figure 4-8. The results of the EM-simulation become closer to the proposed method for the higher frequencies. From these results, we can conclude that the results at higher frequencies than 700 GHz will give closer and comparable results calculated by the proposed method.
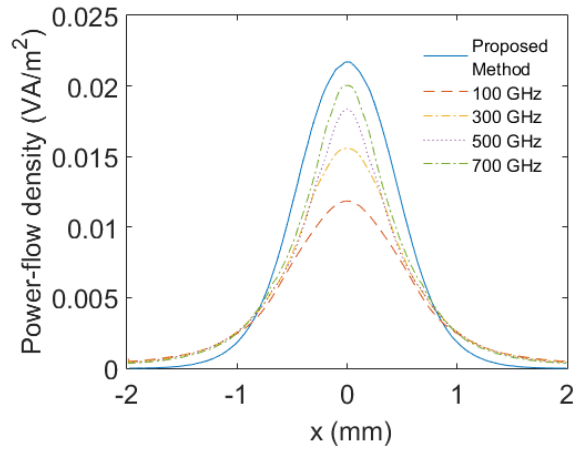
(a)
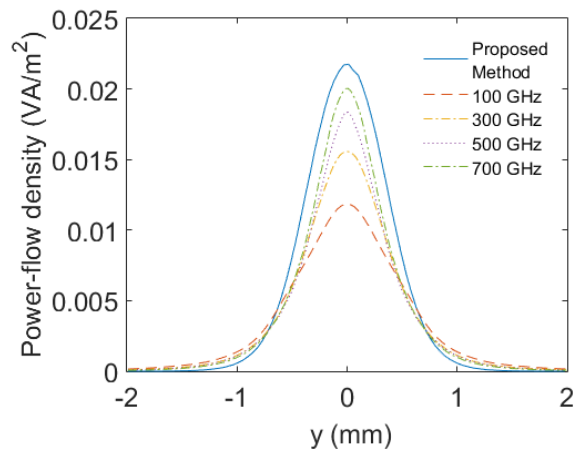
(b)

Figure 4-8 Power flow density distribution comparison calculated with the proposed method and the EM-simulation at plane orthogonal to z-axis at z=0 mm (a) at line y=0 mm and (b) at line x=0 mm.

4.3 Power-flow density distribution at frequency 1 THz

We tried three dimensional (3D) EM simulations at plane wave frequency at 1 THz, but we had a serious problem. This is because the size of the Si-lens is much larger than the wavelength of the THz wave and this condition led to difficulty of

huge calculations, though the 3D calculation by the proposed method can be performed more easily than the EM simulation. Therefore, for comparison at frequency 1 THz, we execute two dimensional (2D) calculations by the proposed method and simulation by the EM-simulation. The 2D calculations by both methods are done under the same condition of THz power-flow-density of incoming radiation with a linear polarization parallel to x-axis and an electric field (rms) of 1 V/m.

Figure 4-9 (a) and (b) are the power flow density distribution calculated by the proposed method on the plane parallel and perpendicular to the polarization of incoming rays, respectively. Figure 4-10 (a) and (b) are the power-flow-density distributions on the plane parallel and perpendicular to the polarization of incoming rays simulated with the EM-simulator, respectively. The power-flow-density distributions calculated by the EM simulator on the planes parallel and perpendicular to the polarization of incoming radiation (Figure 4-10) are similar to the results of Figure 4-9. The rays are converged by the hemispherical boundary, and the power-flow density increases to the focus on z-axis in the Si-lens. The distribution of the power-flow density distribution in Figure 4-9 (a) is wider than that in Figure 4-9 (b), which is consistent with the transmittance distribution shown in Figure 4-1 (a).
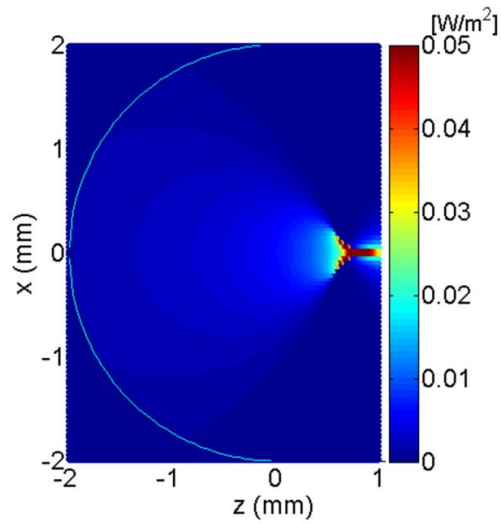
(a)
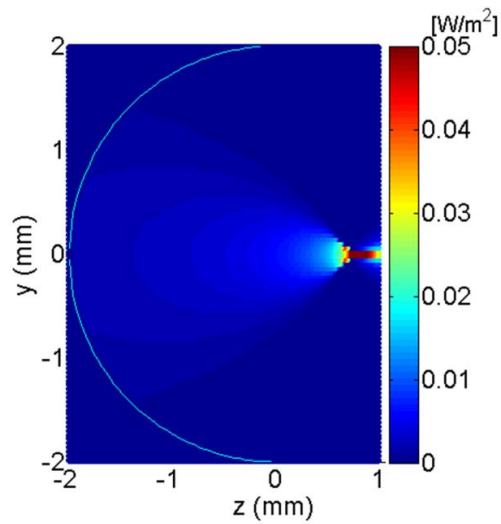
(b)

Figure 4-9 Power-flow-density distributions on the planes (a) parallel and (b) perpendicular to the linear polarization of incoming rays with an electric field of 1 V/m obtained by 2D calculation of the ray-tracing with Fresnel's transmission.
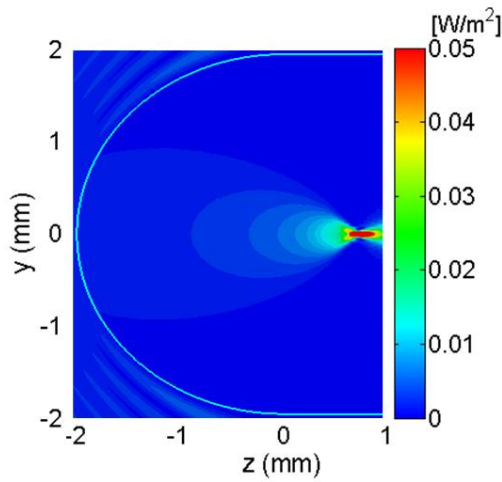
(a)
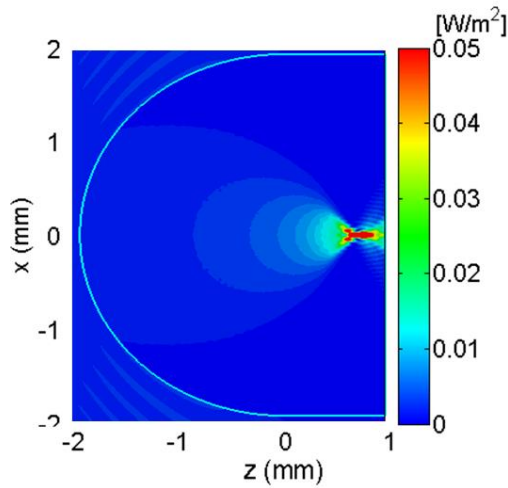
(b)

Figure 4-10 Power-flow density distributions on the planes (a) perpendicular and (b) parallel to the polarization of radiation of incidence, calculated by the EM simulation for uniform radiation of incidence with linear polarization of the x-axis direction and electric field of 1 V/m.

We observed two locations close to the focus: at z=0.4 mm and at z=0.9 mm. Figure 4-11 (a) and (b) show the power-flow-density profiles, which are calculated by the proposed method and the EM-simulation, on the plane parallel to the polarization of incoming radiation at z=0.4 mm and z=0.9 mm, respectively. Figure 4-11 (c) and (d) also show the power-flow-density profiles on the plane

perpendicular to the polarization of incoming radiation at z=0.4 mm and z=0.9 mm, respectively. The THz wave radiation is more converged at z=0.9 mm than at z=0.4 mm, and the power-flow-density profiles on the plane parallel to the incoming polarization are wider than those on the plane perpendicular to the incoming polarization, which is consistent with Figure 4-9 and 4-10. The results of two methods have good agreement on both planes parallel and perpendicular to the polarization of incoming radiation, but the profile of the EM simulation is wider than the proposed ray-tracing with Fresnel's transmission, which is because the proposed method does not include diffraction and the interference of the THz wave in the calculation. Because the dispersion of refractive index and the absorption of high-resistivity silicon are very low in the THz region, our method is valid for estimating the power-flow distribution in the wide frequency range of THz region.

Figure 4-12 is a power-flow-density distribution obtained by three-dimensional (3D) calculation using our proposed method under the same condition of incoming rays as in Figure 4-9. The power-flow-density distributions on planes orthogonal to z-axis at z=0.4 mm and 0.9 mm are shown in Figures 4-12 (a) and (b), respectively. These show that the linearly polarized radiation produces ellipsoidal beam patterns even at converging positions, which is the effect of Fresnel's transmission because the patterns derived by the regular ray-tracing method have circular symmetry for irradiation parallel to the central axis of an optical system. From the above power-flow-density distributions, we can obtain the encircled power in an aperture referred to the total transmitted power as a function of the aperture's radius at z=0.4 mm and 0.9 mm as shown in Figure 4-13 (a) and (b), respectively. Figures 4-14 shows the comparison of the encircled power referred to the total transmitted power as a function of the aperture's radius at z=0.4 mm for incoming linearly polarized rays calculated by our ray-tracing method including Fresnel's transmission and the one obtained by the regular ray-tracing method (Zemax, LLC). In the latter, we adopted a constant transmittance of the normal incidence from air to silicon. This figure displays the results by the regular ray tracing has the error in the transmitted power in comparison with the ray-tracing with Fresnel's transmission. The power transmittance estimated by the proposed method is 68.3% of the input radiation

power; on the other hand the one by the regular ray-tracing is 70.0% of the value for the normal incidence. This shows the proposed method is necessary for executing the precise calculations.

(a)

(b)

(c)

(d)
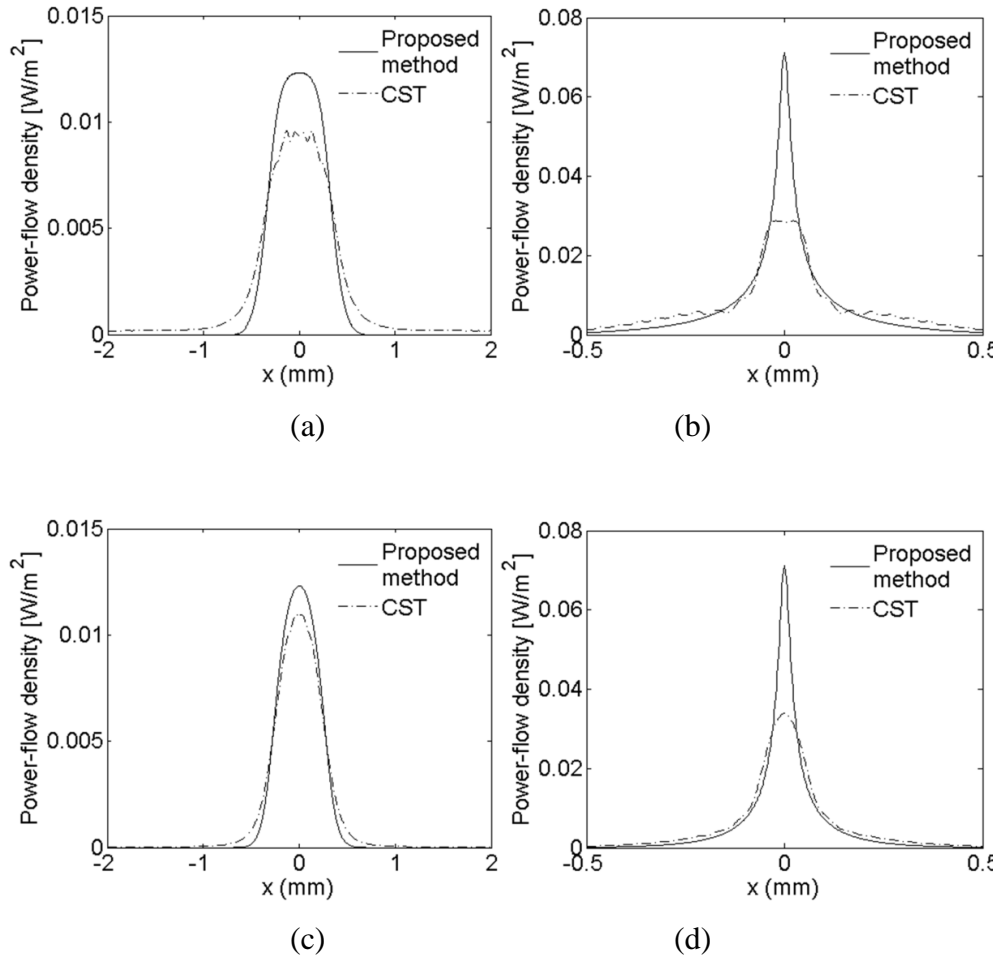
Figure 4-11 Comparison of power-flow-density profiles of 2D calculation by the proposed method with the EM-simulation of CST MW studio. (a) and (b) are the power-flow-density profiles by the two methods on the plane parallel to the polarization of incoming radiation at z=0.4 mm and 0.9 mm, respectively. (c) and (d) are the ones on the plane perpendicular to the polarization of incoming radiation at z=0.4 mm and 0.9 mm, respectively.
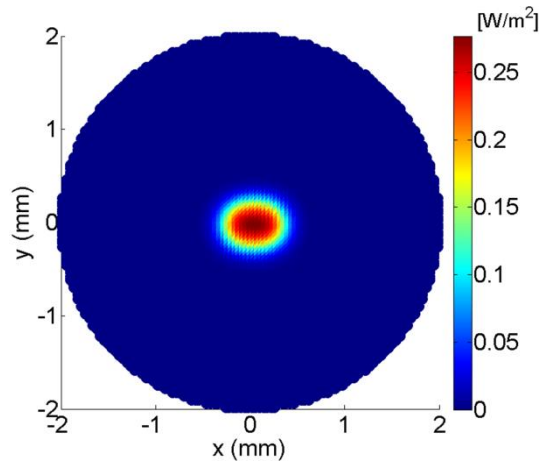
(a)
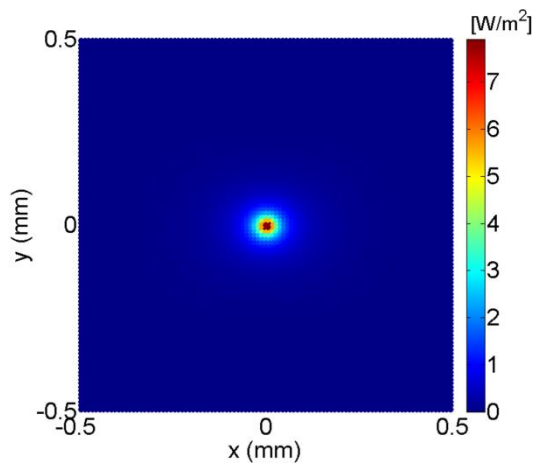
(b)

Figure 4-12 Power-flow-density distributions on planes orthogonal to z-axis obtained by three-dimensional (3D) calculation using our proposed method for the incoming radiation with the linear polarization parallel to x-axis and an electric field of 1 V/m. (a) and (b) are the power-flow-density distributions on planes at z=0.4 mm and 0.9 mm, respectively.
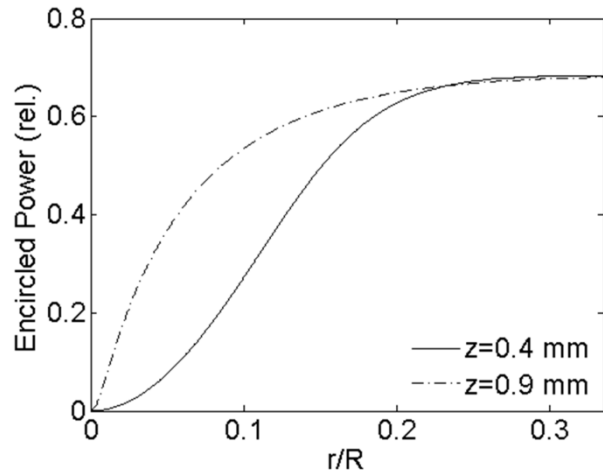
Figure 4-13 Encircled power in an aperture referred to the total transmitted power as a function of the aperture's radius at (a) z=0.4 mm and (b) z=0.9 mm.
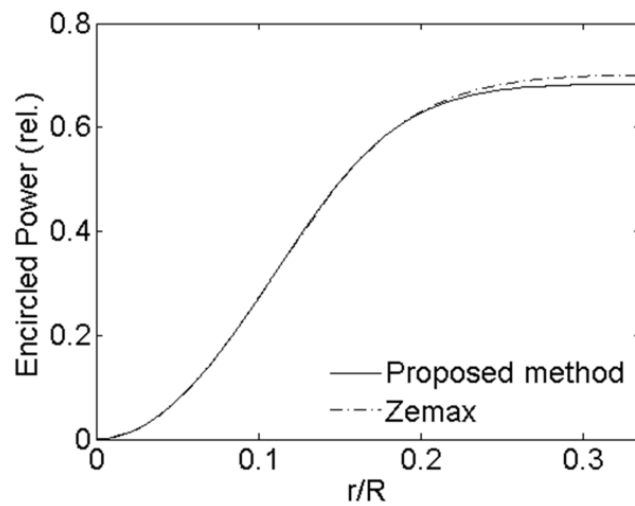
Figure 4-14 Comparison of the encircled power in an aperture referred to the total transmitted power as a function of the aperture's radius at z=0.4 mm for incoming linearly polarized rays calculated by our ray-tracing method including Fresnel's transmission and the one obtained by the regular ray-tracing. The latter assumes a constant transmittance of the normal incidence from air to Si.

4.4 Transmitted power focused in the Si-lens extension

The transmitted power focused in the Si-lens antenna is observed by the transmitted power from the center (z-axis) to the edge of the Si-lens antenna. Term of radii of circles for some percentages are distances determined by summing up the power from the center to the edge of the Si-lens until obtain the determined percentages of the transmited power. Figure 4-15 shows the comparison of the radii of circles for some percentages (50%, 70% and 90%) calculated in the cylinder extension between the proposed method and the regular ray-tracing. By including the Fresnel's transmission, the radii obtained by the proposed method are shorter than the regular ray tracing. This difference shows the power-flow density distribution in the Si-lens antenna irradiated with the linearly polarized THZ wave radiation calculated with the proposed method is more concentrated than the results calculated by the regular ray-tracing.
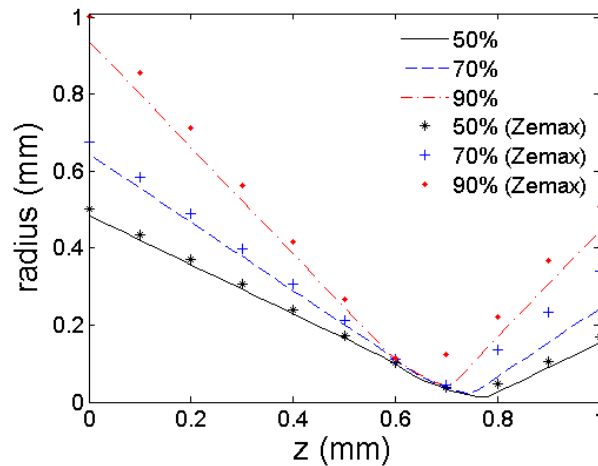
Figure 4-15 Radii of circles for 50%, 70 and 90% of the transmitted power in the cylindrical extension calculated by the ray-tracing with Fresnel's transmission and the regular ray-tracing software (Zemax).

Table 4-1 Location of the focus on the z-axis and length of the radii for some

percentages of the transmitted power calculated by the proposed method

Percentages of transmitted power (%)	z-axis (mm)	Radius (µm)
50	0.78	12.99
60	0.76	14.18
70	0.74	21.45
80	0.72	29.99
90	0.70	39.87
100	0.64	93.41

Table 1 is a summary of the focus position at z-axis and the radii length for six different percentages (50%, 60%, 70%, 80%, 90% and 100%) of the transmitted power. The location of the radii around the focus at the z-axis, where the highest value of the power-flow density distribution, decreases once the percentage increases. The changes of the radii locations are affected by a spherical aberration factor. The spherical aberration occurs because the Si-lens antenna has a hemisphere boundary, which is a large relative aperture; therefore, the focus is no longer a single point. The aperture is a circular are with radius R or the front-view of the Si-lens.

When we design a THz waves detector, such as a THz bolometer, or a THz transceiver antenna, which will be coupled to the Si-lens antenna, the information as shown in Table 1 is useful to find proper size and absorbing pattern (or radiation pattern of an THz antenna) of the THz waves detector or the THz transceiver. The appropriate length of the extended length of the Si-lens antenna and the dimension of THz waves detector or transceiver will improve coupling between the components. Because high-resistivity Silicon has a very low dispersion of refractive

index and low absorption in the THz range, our proposed method is applicable for calculating power-flow density focused by the Si-lens antenna in the wide range of THz region.

CHAPTER 5

EXPERIMENT AND ATTENUATION ANALYSIS OF GLASS AT FREQUENCY 250 GHZ

5.1 Samples of the soda-lime glass

In this section, we discuss samples of the soda-lime glass used in our experiments. Sizes of length and width of the glass are 10 mm and 10 mm, respectively. We prepared five glasses with different thickness: 1 mm, 2 mm, 3 mm, 5 mm and 10 mm. The different thickness are used to identify the attenuated power depending on the glass thickness. To get the real thicknesses, we precisely measured the samples thickness at number of location on their surface by a digital micrometer (Nikon Digi micro MF-501) and calculate the mean thickness and their respective standard deviations. Table 5.1 is a summary of the measurement data. From this measurement, the thickness from the thinnest glass to the thickest glass are 1.003 ± 0.003 mm, 1.883 ± 0.002 mm, 2.837 ± 0.002 mm, 4.834 ± 0.003 mm and 9.872 ± 0.003 mm. The absolute uncertainties of the measured thickness are relatively small, which meant that the glasses have uniform thickness. In the next discussion, we use the mean thickness for analysis of the glass attenuation.

Table 5-1 Summary of the glass thickness measured by using Nikon Digi micro MF-501

	Glass Thickness (mm)				
Min	1.001	1.881	2.835	4.832	9.870
Median	1.003	1.883	2.837	4.833	9.872
Max	1.007	1.885	2.839	4.837	9.875
Mean	1.003	1.883	2.837	4.834	9.872
STD	0.00183303	0.001345	0.001234	0.001159	0.001607

5.2 Refractive index measurement with a transmission THz-TDS Measurement

In our first measurement, we use a transmission THz Time Domain Spectroscopy (THz-TDS) system to measure refractive index of the glass in the THz region. The THz-TDS system is same as used in the reference [16] [56]. Figure 5-1 shows a schematic configuration of the transmission-type THz-TDS system. A THz wave emitter is low temperature gallium arsenide photoconductive (LT-GaAs PC) antenna, and the detection of the THz wave is done with a zinc telluride (ZnTe) crystal through electro-optic (EO) effect. Dry nitrogen (N_2) filled the space where the THz waves emitted, transmitted and detected. When the measurement are conducted, the glass sample is placed in a sample holder. In this measurement, size (length x width) and thickness of the sample are 20 mm x 20 mm and 1.883 mm, respectively.
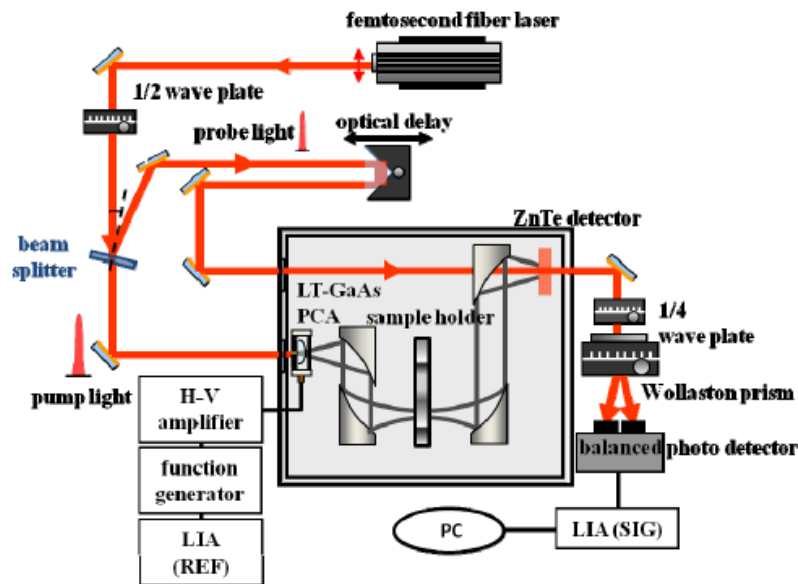
Figure 5-1 Schematic of the transmission THz-TDS system **[56]**.

During the measurement, the THz-TDS records a time-domain pulse of THz electric field in two conditions: a sample signal passing through the sample under investigation and a reference signal in the absence of the sample. Figure 5-2 (a) and (b) show the reference signal and the sample signal recorded with the THz-TDS system, respectively. Peak amplitude of the sample signal as shown in Figure 5-2 (b) is lower than the reference signal as in Figure 5-2 (a). This is meaning that the THz wave power is attenuated when propagating in the glass. The time domain sample signal is delayed due to the optical path length become longer when the pulse propagating in the sample.

After the reference signal and the sample signal were measured by using the THz-TDS system, the two signals are used to analyze the glass refractive index. In order to determine the refractive index, the signals are converted to frequency-domain by using a standard calculation of fast Fourier transformation (FFT) to obtain intensity and phase spectra. These spectra are processed further to calculate the refractive index. Theoretical explanation of this procedure can be found in reference [16]. Figure 5-3 shows the refractive index and its standard deviation in the THz range frequency analyzed from the two time domain signals. Figure 5-3 shows that the refractive indices measured with the THz-TDS system are reliable from 0.2 THz to 1 THz, which allow the glass to works in a wide frequency range. The refractive index at 250 GHz, which is around 2.715, is considered in the next section to analyze the glass attenuation. The refractive index is higher than its refractive index at optics, which is around 1.52.
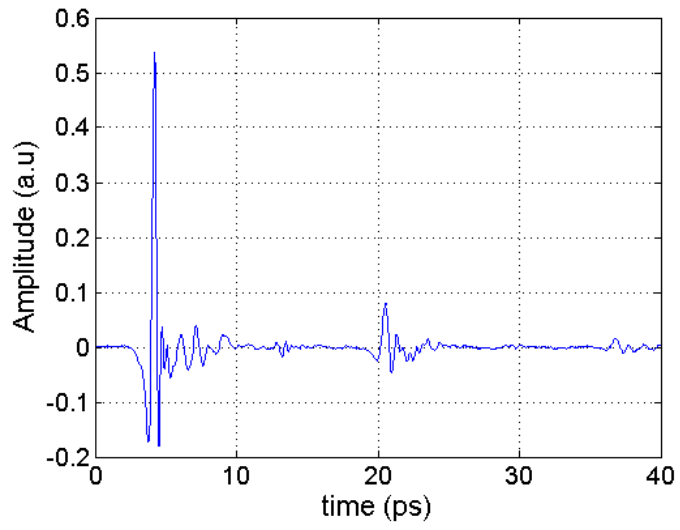
(a)
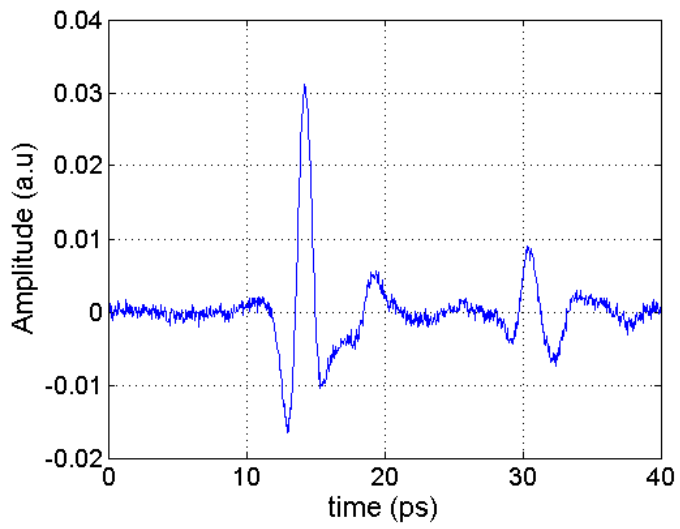
(b)

Figure 5-2 THz time domain signal of (a) the reference signal and (b) the sample
signal measured with the transmission THz-TDS.
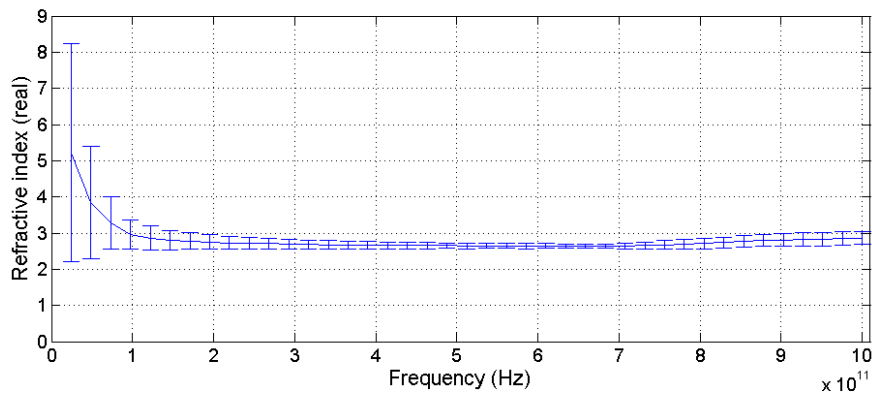
Figure 5-3 Refractive index and standard deviation analyzed from the measured data of the transmission THz time domain spectroscopy

5.3 THz wave measurement with a THz pyro detector

After we obtained the refractive index measured with the THz-TDS, the first measurement for the THz waves passed through the samples is conducted by using a pyro detector of SPH-CM-Test (made by Spectrum Detector Inc.). Figure 5-5 is a schematic of measurement setup to measure the THz waves by using the pyro detector. A THz wave source is prepared by using Anritsu MG3692C RF/Microwave Signal Generator (13.2778 GHz, +10 dBm) combined with a frequency multiplier of VDI Amplifier/Multiplier (x 18, VDI, WR 3.4). Information for the others equipment is summarized in Table 5-2.
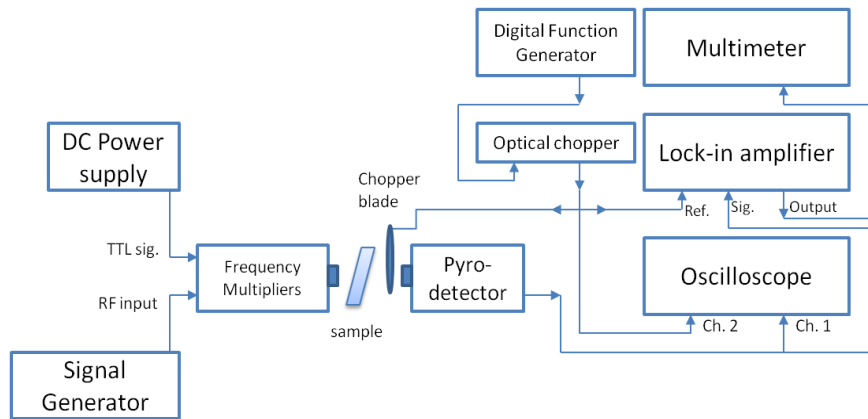
Figure 5-4 A schematic of measurement setup with the pyrodetector to measure the THz wave passed through the glass sample.

Table 5-1 Equipments used in the THz wave measurement with the pyrodetector

Equipment	Type
DC power supply	Kenwood PR18-1.2A regulated DC power supply
Signal generator	Anritsu MG3692C RF/Microwave signal generator
Frequency multiplier	VDI amplifier/multiplier chain + WR 3.4
Optical chopper system	ThorLabs optical chopper
Pyro detector	SPH-CM-Test (made by Spectrum Detector Inc.)
Oscilloscope	LeCroy WaveAce 102 Oscilloscope
Lock-in amplifier	SR510 Lock-in amplifier Stanford research systems
Digital function generator	NF digital function generator 0.1 mHz-2 MHz DF 1906

During the measurement for every glass sample, the sample is placed in between the THz wave source and the pyro detector. Beams of the THz waves from the THz wave source is irradiated to the sample. After the THz waves passing through the glass sample, the transmitted THz waves are chopped with an optical chopper and then detected by the pyro detector. The detected THz waves is

connected to a lock-in amplifier. The chopper signal is also used as a reference signal connected to the lock-in amplifier. The output is measured with a multi meter. The measurement is conducted at room temperature and atmospheric pressure. An angle of inclination of the glass sample as shown in Figure 5-5 is applied to avoid the THz waves reflected back to the THz source. The inclination angle should be considered because it affect the optical path length inside the glass. The angle of inclination of one glass is different to the others depending on its thickness. The angles of inclination from the thinnest to the thickest are $18^{o}\pm0.5^{o}$, $17^{o}\pm0.5^{o}$, $16^{o}\pm0.5^{o}$, $14^{o}\pm0.5^{o}$ and $9^{o}\pm0.5^{o}$.

Before we measure the THz waves passed to the samples, we measure the THz waves detected directly by the pyro detector without passing through the glasses to get a reference signal. The reference signal is used to calculate transmittance of the THz waves detected with the pyro detector after passing through the glass samples. The measurement data (Table 5-2) shows that the power level of the detected signal decreases when the thickness of the glass increases, which meant attenuation occurs when the signal travelling in the glass. The detected signal of one glass is bigger than two glasses, even have totally the same thickness. The decreasing of the detected power when the THz wave passing through two glasses is possibly affected by the amount of transmittance and reflectance between air and the glass on the two glasses configuration is more than the one glass. Other factor that possibly affect the detected signal is the angle of inclination (θ). When the angle of inclination (θ) increases, the thickness of the glass passed through by the THz wave also increases. For a polarized incoming radiation, the angle of inclination (θ) is also a variable to calculate the transmittance and the reflectance. In the next discussion, we consider these factors in the attenuation analysis.

Table 5-2 Experiment data of the THz waves passing through the glass measured
with the pyro detector

Glass thickness 'd' (mm)	Signal (mV)
None	4.677
1	2.795
1+1	1.118
2	1.173
2+1	0.501
3	0.631
2+3	0.129
5	0.261
10	0.065

5.4 THz wave measurement with a body scanner system

The second measurement for the THz waves passed through the samples is conducted by using a body scanner system provided by KSK Corporation. Schematic of this measurement setup is shown in Figure 5-7. The glasses are placed between the THz wave source and the body scanner. The body scanner measures intensity of the THz waves in images. Levels of the detected power are determined with different brightness of the images. For every measurement for different thickness of the glass, mean of the measurement data and its standard deviation are used for the attenuation analysis.
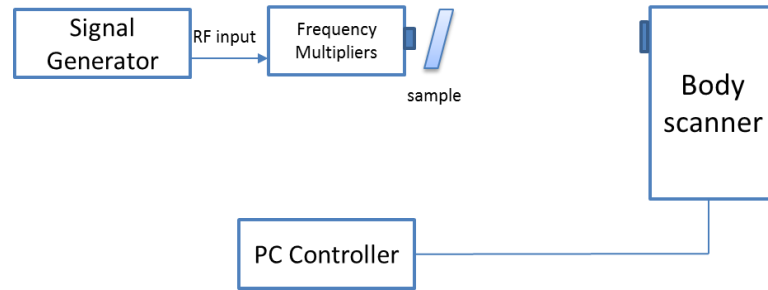
Figure 5-5 A schematic of measurement setup to measure the THz waves with the body scanner

5.5 Attenuation calculation using data measured with the pyro detector by least square fit to an arbitrary function

In order to determine the glass attenuation, the THz waves measured with the pyro detector are analyzed with nonlinear regression analysis. Transmittance levels are calculated from ratio between the THz waves passed through the glass and the THz waves detected without passed through the glass. In order to do the attenuation analysis, we derive a transmittance function depend on the refractive index, a transmittance, a reflectance, and the angles of incidence. Figure 5-6 shows a schematic of a ray of incidence, rays of reflection, rays of transmission and multi-reflection in a glass with a thickness d. Once a ray of incidence comes from medium 1 (refractive index of n_1) to medium 2 (refractive index of n_2), the ratio of the power reflected back to medium 1 to the power of incidence and the ratio of the power transmitted to medium 2 to the power of incidence are calculated as reflectance (T_1) and transmittance (R_1), respectively. After the transmitted ray traveling in the glass reaches the second boundary, the reflectance (R_1) and the transmittance (T_1) are also occur, which have the same value when the ray come from medium 1 to medium 2. Those reflections inside the glass is named as a multi-reflection phenomenon.
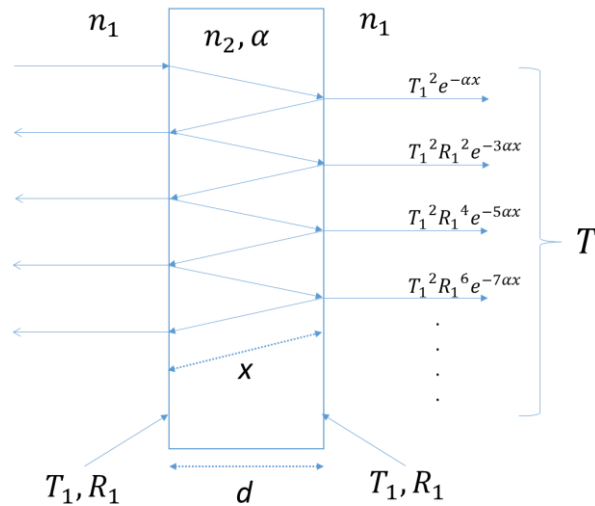
Figure 5-6 A schematic of a ray of incidence, rays of reflection, rays of transmission and multi-reflection in a glass with thickness d.

An angle of inclination of the glass sample as shown in Figure 5-5 is applied to avoid the THz waves reflected back to the THz wave source. When the angles of inclination (θ) are more than zero degree, the optical path length inside the glass will increase and become longer than the sample thickness (d). The optical path length affected by the angles of inclination can be estimated by Equation 5-1. From the measured thickness of the glasses and the maximum angle of inclination, the maximum optical path length calculated with Equation 5-1 from the thinnest to the most thickness of the glasses are 1.007 mm, 1.894 mm, 2.852 mm, 4.853 mm and 9.889 mm.

$$x = \frac{d}{\cos\left(\sin^{-1}\left(\frac{n_1 \sin\theta}{n_2}\right)\right)} \qquad\qquad (5\text{-}1)$$

The transmittances are also affected by the THz wave polarization. If the THz wave polarization is parallel to the plane of incidence, the transmittance increases as the angle of incidence increases until reach Brewster's angle as discussed in the Chapter 2. If the THz waves polarization is perpendicular to plane of incidence, the transmittance decreases as the angle of incidence increases. Figure 5-7 shows the

transmittance, both the parallel polarization (T_p) and the perpendicular polarization (T_s), for linearly polarized wave traveling from the medium 1 $(n_1 = 1)$ to the medium 2 $(n_2 = 2.715)$. Figure 5-7 shows that the Brewster's angle is located at 70° for the parallel polarization. According to the output window of the frequency multiplier and orientation of the angle of inclination, the transmittance (T_1) and the reflectance (R_1) are calculated with Equation 5-2 and 5-3, respectively, which the THz wave polarization vector is perpendicular to the plane of incidence. Information of refractive indices (n_1, n_2), an angle of incidence (θ_i) and an angle of transmission (θ_t) are needed to calculate the transmittance and the reflectance. Refractive index of medium 1 is refractive index of air $(n_1=1)$. Refractive index of medium 2 is refractive index of the glass obtained from the THz-TDS measurement $(n_1 = 2.715$ at frequency 250 GHz). The angle of incidence (θ_i) is the angle of inclination (θ) depend on how the sample placed in the measurement. The angle of transmission (θ_t) is calculated with Snell's law of refraction.
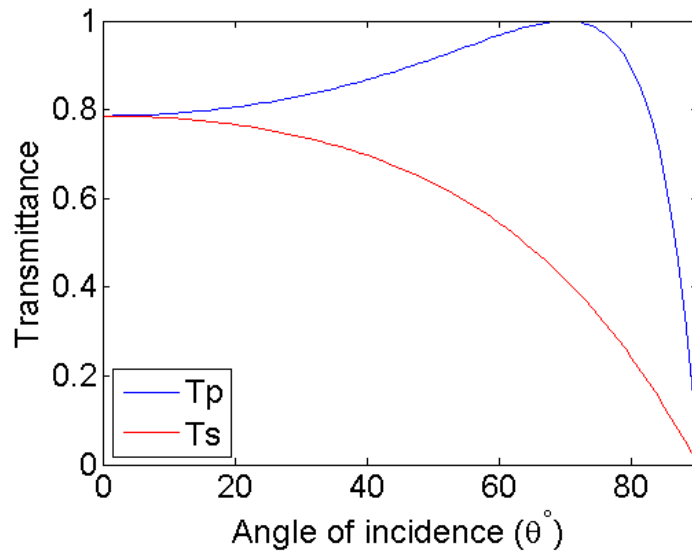
Figure 5-7 Transmittance from air $(n_1=1)$ to the glass $(n_2=2.715)$ as a function of angles of incidence. Tp and Ts are transmittance of the incoming radiation whose polarization are parallel and perpendicular to the plane of incidence, respectively.

$$R_1 = \left|\frac{n_1 cos\theta_i - n_2 cos\theta_t}{n_1 cos\theta_i + n_2 cos\theta_t}\right|^2 \qquad\qquad (5\text{-}2)$$

$$T_1 = 1 - R_1 \qquad\qquad (5\text{-}3)$$

As shown in Figure 5-6, the total power of the transmitted THz waves is the summing of the power transmitted from medium 2 to the medium 1 which travels in the right direction. Equation 5-4 is a derivation of the total transmitted power, which is depend on the transmittance (T_1), the reflectance (R_1) and the optical path length (x).

$$T = \frac{T_1{}^2 e^{-\alpha x}}{1 - R_1{}^2 e^{-2\alpha x}} \qquad\qquad (5\text{-}4)$$

To find a solution for Equation 5-4, we can use Least Square Fit to an arbitrary function including experiment data of the pyro detector [57]. To simplify Equation 5-4 into one coefficient of the glass attenuation (α), we can use the refractive index glass, which were measured by the transmission THz-TDS system. Therefore, the solution for the glass attenuation (α) can be calculated statistically by using the THz wave measurement data for the dependent variable of T and the glass thickness for the independent variable of x.

$$\chi^2 \equiv \sum_i \left(\frac{\Delta y_i}{\sigma_i}\right)^2 \qquad\qquad (5\text{-}5)$$

If $\sigma_i = \sigma$

$$\chi^2 = \sum_i \left(\frac{\Delta y_i}{\sigma}\right)^2 = \frac{1}{\sigma^2}\sum_i(\Delta y_i)^2$$

$$\sigma^2\chi^2 = \sum_i(\Delta y_i)^2 = \sum_i\big(y_i - y(x_i)\big)^2 \qquad (5\text{-}6)$$

Chi-square (χ^2) in Equation 5-5 is a statistic which characterizes the dispersion of the observed data from the expected data. The numerator of Equation 5-5 is a measure of the spread of the observations; the denominator is a measure of the expected spread. Least-squares fitting procedure is done by minimizing χ^2 with respect to each of the coefficient. The minimum value of the function of Equation 5-5 expanded into Equation 5-6 is one which yields a value of 0 for the partial derivatives with respect to each of the coefficients. Because we want to solve the coefficient of α, the partial derivatives of Equation 5-6 with respect to coefficient α (Equation 5-7) should be solved.

$$\frac{\delta}{\delta\alpha}\sigma^2\chi^2 = \frac{\delta}{\delta\alpha}\left[\sum_i\left(y_i - y(x_i)\right)^2\right] = 0 \qquad (5\text{-}7)$$

We use the statistical method of least square fit to an arbitrary function to analyze the measurement data of the pyro detector. We consider the total transmittance equations (Equations 5-4) and the glass refractive index measured with the transmission THz-TDS system to calculate the glass attenuation. We utilize Matlab Curve Fitting Tool to make a fit plot and to calculate the glass attenuation. As a comparison, we calculate the glass attenuation as a function of the glass thickness by using an exponential function analysis without consider the transmittance factor.

5.6 Attenuation calculation using data measured with the body scanner by Least Square Fit to a linear function

Data analysis of the measurement data obtained with the body scanner measurement are conducted for the detected signal in form of images. Figure 5-8 shows two sample images captured with the body scanner. The brightness levels in those images show the levels of the power detected by the body scanner depend on the glass thickness. An area around center with low scale is an area of beam covering the THz wave source. Those areas of the images captured from varying the glass configuration are analyzed to obtain the glass attenuation. Mean and

standard deviation are two parameter considered in the attenuation analysis. The transmitted power levels are determined by differences between mean of the measurement data, which is the area covering beams of the THz wave source, and a reference data as defined in Equation 5-8. The reference data is the background data or the area where the beams of the THz wave source is not covered. Equation 5-9 is an exponential equation to calculate the attenuation coefficient (α). Equation 5-10 is a modification of Equation 5-9 to simplify the attenuation analysis by the statistical method of least square fit to a linear function. To get the proper standard deviation data from the measurement needed for the attenuation analysis, Equation 5-11 is used to transform the standard deviation, which is initially described in Equation 5-8.

(a)   (b)
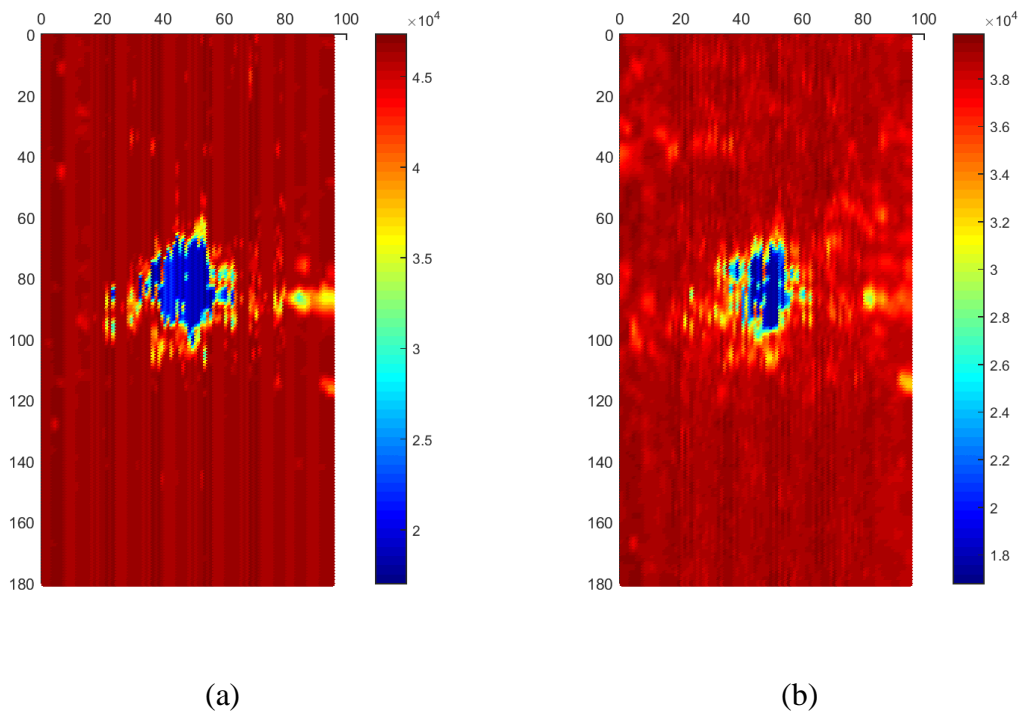
Figure 5-8 Sample images measured with the body scanner from three glass configuration which the total thickness of (a) 6.854 mm and (b) 8.689 mm, respectively.

$$y = u - v \rightarrow \sigma_y{}^2 = \sigma_u{}^2 + \sigma_v{}^2 \qquad (5\text{-}8)$$

$$y = ce^{-\alpha x} \qquad (5\text{-}9)$$

$$Y = \ln y = \ln c - \alpha x \qquad (5\text{-}10)$$

$$Y = \ln(y) \rightarrow \sigma_Y = \frac{\sigma_y}{y} \qquad (5\text{-}11)$$

Equation 5-12 is a general linear function to apply the least-squares fitting to linear function. Equation 5-10 has same form with Equation 5-12. Least square fit to a linear function (Equation 5-12) is used to analyze the attenuation factor $(b = \alpha)$ of the glasses. Equation 5-13 – 5-15 are coefficients of the least-squares fitting. Uncertainties of the coefficients are formulated in Equations 5-16 and 5-17.

$$y(x) = a + bx \qquad (5\text{-}12)$$

$$a = \frac{1}{\Delta}\left(\sum \frac{x_i{}^2}{\sigma_i{}^2} \sum \frac{y_i}{\sigma_i{}^2} - \sum \frac{x_i}{\sigma_i{}^2} \sum \frac{x_i y_i}{\sigma_i{}^2}\right) \qquad (5\text{-}13)$$

$$b = \frac{1}{\Delta}\left(\sum \frac{1}{\sigma_i{}^2} \sum \frac{x_i y_i}{\sigma_i{}^2} - \sum \frac{x_i}{\sigma_i{}^2} \sum \frac{y_i}{\sigma_i{}^2}\right) \qquad (5\text{-}14)$$

$$\Delta = \sum \frac{1}{\sigma_i{}^2} \sum \frac{x_i{}^2}{\sigma_i{}^2} - \left(\sum \frac{x_i}{\sigma_i{}^2}\right)^2 \qquad (5\text{-}15)$$

$$\sigma_a{}^2 \simeq \frac{1}{\Delta}\sum \frac{x_i{}^2}{\sigma_i{}^2} \qquad (5\text{-}16)$$

$$\sigma_b{}^2 \simeq \frac{1}{\Delta}\sum \frac{1}{\sigma_i{}^2} \qquad (5\text{-}17)$$

5.7 Results and discussion

In the pyro detector measurement data, Figure 5-9 shows the transmittances, which are determined as the ratio between the THz wave power passed through the glass and the power detected directly without passing through the glass. Figure 5-9 and Figure 5-10 show the fitting plot to an exponential function and the function described in Equation 5-4, respectively. The attenuation analyzed from the pyro detector measurement data are around 0.556 mm^{-1} and 0.492 mm^{-1} when the analysis conducted without and with consider the Fresnel's factor, respectively. The lower attenuation level in Figure 5-10 is caused by the transmission and the reflection occur in the boundary between the glass and air. These factors have a contribution to reduce the transmitted power. Therefore, the attenuation analysis in Figure 5-10 is lower than in Figure 5-9 for the same detected power.
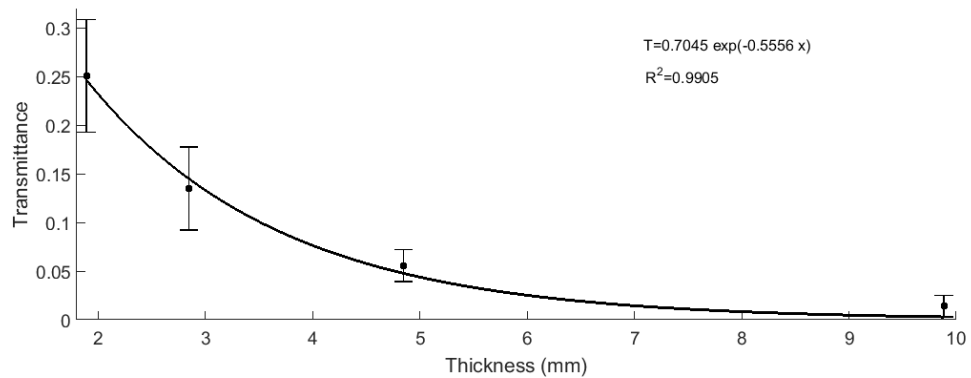
Figure 5-9 Transmittance measured with the pyro detector and fitting plot to an exponential function without consider Fresnel's transmission and reflection.
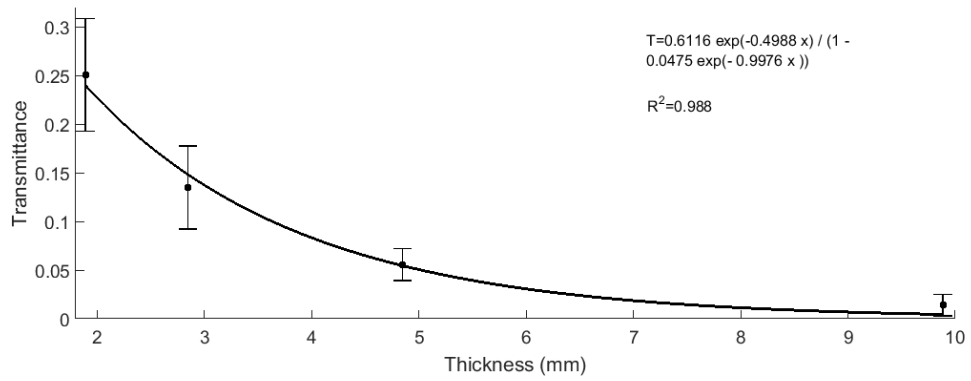
Figure 5-10 Transmittance measured with the pyro detector and fitting plot to the function of Equation 5-4 consider Fresnel's transmission and reflection.

In the body scanner measurement data, the signals are determined as the differences between means of the beams area and means of the background. Figure 5-11 shows the measurement data and its fitting plot to a linear function of Equation 5-11 which not to include the Fresnel's factors. The attenuation is around 0.574 mm^{-1} which is close to and clarify the pyro detector result.
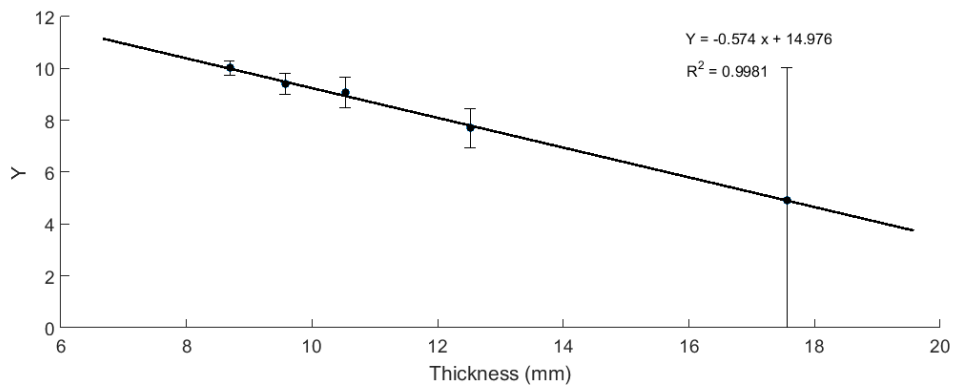
Figure 5-11 Signals measured with the body scanner and fitting plot to a linear function.

The attenuation analysis from the data measured with the pyro detector as well as the body scanner show that the THz wave is attenuated around half for every one millimeter thickness of the glass. After we obtain the glass attenuation, we can estimate the attenuated power and the reflected power. Figure 5-11 shows an estimation of the transmittance, the reflectance and the attenuated power (in ratio to the initial emitted power).
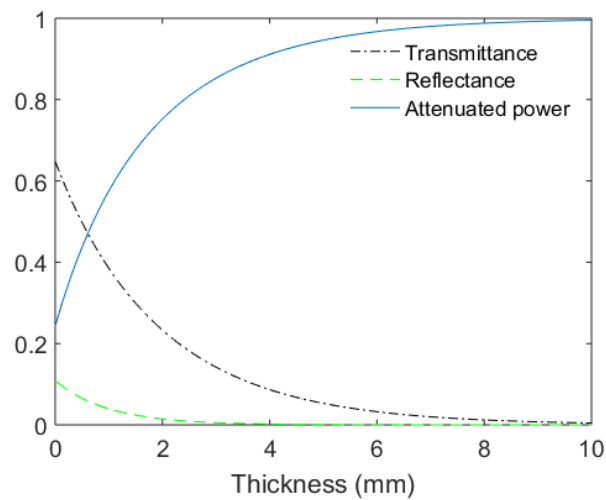
Figure 5-12 Estimation of transmittance, reflectance and attenuated power of the glass as a function of the thickness.

CHAPTER 6
CONCLUSION

We calculate and display the 3D power-flow-density distribution in an extended hemispherical Si-lens by the proposed ray-tracing method including Fresnel's transmission for incoming THz rays with linear polarization. Our proposed method is consistent with the electromagnetic simulation except for the effect of diffraction and interference. Our method has advantages over the EM simulation in simplicity and convenience and over the regular ray-tracing in terms of preciseness in the calculation of the transmitted power-flow density in optical systems using Si-lens antennas. Because both dispersion of refractive index and absorption in high-resistivity Silicon are very low in the THz region, our proposed method is valid for estimating the power-flow-density distribution in the wide frequency range of THz region. The ray-tracing method with Fresnel's transmission will contribute to designing optical elements like dielectric lens antennas in THz quasi-optical systems.

We have measured and analyzed optical characteristics of refractive index and attenuation of soda-lime glass at frequency 250 GHz. The study of soda-lime glass attenuation at frequency 250 GHz is conducted by using measurement data obtained from the three measurement setup: the THz signal measurement with pyro detector, the THz signal measurement with body scanner system and the refractive index measurement with transmission THz time domain spectroscopy (THz-TDS) system. The refractive index measurement shows that the refractive index of the glass has low diffraction between 0.2 – 1 THz, therefore, the glass can provide an attenuation element for a wide range frequency. The refractive index (around 2.715 at frequency 250 GHz) is higher than its refractive index at optics which is around 1.52. The glass attenuation analyzed from the pyro detector measurement data are around 0.556 mm^{-1} and 0.4988 mm^{-1} when the analysis conducted without and with consider the Fresnel's factor, respectively. The attenuation analyzed from the body scanner measurement without consider the Fresnel's factor is around 0.574 mm^{-1},

which is close to the pyro detector result. The results show that the glass is a potential and low cost material to reduce until half of THz wave power for every 1 mm.

REFERENCES

[1] B. Furguson and X. Zhang, "Materials for terahertz science and technology," *Nature Materials,* vol. 1, no. 1, pp. 26-33, 2002.

[2] C. M. Armstrong, "The truth about terahertz," *Spectrum, IEEE,* vol. 49, no. 9, pp. 36 - 41, 27 September 2012.

[3] G. Mourou, C. Stancampiano, A. Antonetti and A. Orszag, "Picosecond microwave pulses generated with a subpicosecond laser-driven semiconductor switch," *Applied Physics Letters,* vol. 39, p. 295, 1981.

[4] N. Kapowicz, H. Zhong, C. Zhang, K.-I. Lin, J.-S. Hwang, J. Xu and X.-C. Zhang, "Compact continuous-wave subterahertz system for inspection applications," *Applied Physics Letters,* vol. 86, p. 054105, 28 January 2005.

[5] C. Yu, S. Fan, Y. Sun and E. Pickwell-MacPherson, "The potential of terahertz imaging for cancer diagnosis: A review of investigations to date," *Quantitative Imaging in Medicine and Surgery,* vol. 2, no. 1, pp. 33-45, 2012.

[6] C. Jördens and M. Koch, "Detection of foreign bodies in chocolate with pulsed terahertz spectroscopy," *Optical Engineering,* vol. 47, no. 3, p. 037003, 20 March 2008.

[7] A. Gowen, C. Sullivan and C. O'donnel, "Terahertz time domain spectroscopy and imaging: Emerging techniques for food process monitoring and quality control," *Trends in Food Science and Technology,* vol. 25, no. 1, pp. 40-46, 2012.

[8] G. Ok, K. Park, H. S. Chun, H.-J. Chang, N. Lee and S.-W. Choi, "High-performance sub-terahertz transmission imaging system for food inspection," *Biomedical Optics Express,* vol. 6, no. 5, pp. 1929-1941, 2015.

[9] A. Fitzgerald, B. Cole and P. Taday, "Nondestructive analysis of tablet coating thicknesses using terahertz pulsed imaging," *Journal of Pharmaceutical Sciences,* vol. 94, no. 1, p. 177–183, January 2005.

[10] I. Takeuchi, K. Shimakura, H. Ohtake, J. Takayanagi, K. Tomoda, T. Nakajima, H. Terada and K. Makino, "Nondestructive Analysis of Structure and Components of Tablet Coated with Film by the Usage of Terahertz Time-Domain Reflection Spectroscopy," *Journal of Pharmaceutical Sciences,* vol. 103, no. 1, pp. 256-261, 2014.

[11] M. Nagel, P. H. Bolivar, M. Brucherseifer, H. Kurz, A. Bosserhoff and a. R. Büttner, "Integrated THz technology for label-free genetic diagnostics," *Applied Physics Letters,* vol. 80, no. 1, pp. 154-156, 7 January 2002.

[12] R. Piesiewicz, T. Kleine-Ostmann, N. Krumbholz, D. Mittleman, M. Koch, J. Schoebel and T. Kurner, "Short-Range Ultra-Broadband Terahertz Communications: Concepts and Perspectives," *IEEE Antennas and Propagation Magazine,* vol. 49, no. 6, pp. 24-39, 2007.

[13] H.-j. Song and T. Nagatuma, "Present and Future of Terahertz Communications," *IEEE Transactions on Terahertz Science and Technology,* vol. 1, no. 1, pp. 256-263, 2011.

[14] M. Aoki, M. Takeda and N. Hiromoto, "Electromagnetic Simulation for THz Antenna-Coupled Microbolometers Operated at Room Temperature," *Makara Journal of Technology ,* vol. 17, no. 1, pp. 1-6, 2013.

[15] R. F. Potter, "Germanium (Ge)," in *Handbook of Optical Constants of Solids*, Florida, Academic Press, Inc. , 1985, p. 478.

[16] S. R. Tripathi, M. Aoki, M. Takeda, T. Asahi, I. Hosako and N. Hiromoto, "Accurate Complex Refractive Index with Standard Deviation of ZnTe Measured by Terahertz Time Domain Spectroscopy," *Japanese Journal of Applied Physics,* vol. 52, no. Number 4R, April 2013, p. 042401, 11 March 2013.

[17] E. D. Palik, "Gallium Arsenide (GaAs)," in *Handbook of Optical Constants of Solids*, Florida, Academic Press, Inc. , 1985, p. 443.

[18] E. D. Palik, "Lithium Niobate (LiNbO3)," in *Handbook of Optical Constants of Solids*, Florida, Academic Press, Inc. , 1985, p. 702.

[19] A. Borghessi and G. Guizetti, "Gallium Phosphide (GaP)," in *Handbook of Optical Constants of Solids*, Florida, Academic Press, Inc. , 1985, p. 464.

[20] J. Ashok and P. L. H. Varaprasad, "Polyethylene (C2H4)n," in *Handbook of Optical Constants of Solids II*, California, Academic Press, Inc., 1991, p. 985.

[21] "TYDEX," [Online]. Available: http://www.tydexoptics.com/pdf/THz_Materials.pdf. [Accessed 2 July 2015].

[22] Y.-S. Jin, G.-J. Kim and S.-G. Jeon, "Terahertz Dielectric Properties of Polymers," *Journal of the Korean Physical Society,* vol. 49, no. 2, pp. 513-517, 2006.

[23] "Broadband, Inc.," [Online]. Available: http://www.bblaser.com/pdf/THzSuperLens_ver3.pdf. [Accessed 2 July 2015].

[24] C. Ronne, L. Thrane, P. Astrand, K. Mikkelsen and S. Kediding, "Investigation of the temperature dependence of dielectric relaxation in liquid water by THz reflection spectroscopy and molecular dynamics simulation," *The Journal of Chemical Physics,* vol. 107, p. 5319, 1997.

[25] S. M. Sze and K. K. NG., Physics of Semiconductor devices 3rd edition, New Jersey: John Wiley & Sons, Inc. , 2006.

[26] P. F. Goldsmith, Quasioptical Systems: Gaussian Beam Quasioptical Propagation and Applications., Wiley-IEEE Press, 1998.

[27] D. B. Rutledge, D. P. Neikirk and D. P. Kasilingam, Integrated-Circuit Antennas, vol. 10, New York: Academic Press, 1983, pp. 1-90.

[28] M. Kominami, D. M. Pozar and D. H. Schaubert, "Dipole and Slot Elements and Arrays on Semi-Infinite Substrates," *IEEE Transactions on Antennas and Propagation,* Vols. AP-33, no. 6, pp. 600-607, 1985.

[29] D. F. Filipovic, S. S. Gearhart and G. M. Rebeiz, "Double-Slot Antennas on Extended Hemispherical and Elliptical Silicon Dielectric Lenses," *IEEE Transactions on Microwave Theory and Techniques,* vol. 41, no. 10, pp. 1738-1749, October 1993.

[30] C. Apriono and E. T. Rahardjo, "Radiation Characteristics of a Planar Strip Dipole Antenna and a Slot Dipole Antenna for THz Applications," *MAKARA Journal of Technology Series,* vol. 17, no. 3, pp. 138-144, 2013.

[31] D. B. Rutledge and M. S. Muha, "Imaging Antenna Arrays," *IEEE Transactions on Antennas and Propagation,* Vols. AP-30, no. 4, pp. 535-540, 1982.

[32] C. R. Brewitt-Taylor, D. J. Gunton and H. D. Rees, "Planar Antennas on A Dielectric Surface," *Electronics Letters,* vol. 17, no. 20, pp. 729-731, 1981.

[33] F. Formanek, M.-A. Brun, T. Umetsu, S. Omori and A. Yasuda, "Aspheric silicon lenses for terahertz photoconductive antennas," *Applied Physics Letters,* vol. 94, no. 2, p. 021113, 2009.

[34] C. Fattinger and D. Grischkowsky, "Terahertz beams," *Applied Physics Letters,* vol. 54, no. 6, p. 490, 1989.

[35] D. Filipovic, G. Gauthier, S. Raman and G. Rebeiz, "Off-axis properties of silicon and quartz dielectric lens antennas," *IEEE Transactions on Antennas and Propagation,* vol. 45, no. 5, pp. 760-766, 1997.

[36] W. B. Dou and Z. L. Sun, "Ray tracing on extended hemispherical and elliptical silicon dielectric lenses," *International Journal of Infrared and Millimeter Waves,* vol. 16, no. 11, pp. 1993-2002, 1 November 1995.

[37] M. Alonso-delPino, "Design Guidelines for a Terahertz Silicon Micro-Lens Antenna," *Antennas and Wireless Propagation Letters,* vol. 12, pp. 84 - 87, 15 Januari 2013.

[38] T. Nitta, M. Naruse, Y. Sekimoto, K. Mitsui, N. Okada, K. Karatsu, M. Sekine, H. Matsuo, T. Noguchi, Y. Uzawa, M. Seta and N. Nakai, "Beam Pattern Measurements of Millimeter-Wave Kinetic Inductance Detector Camera With Direct Machined Silicon Lens Array," *Terahertz Science and Technology, IEEE Transactions on,* vol. 3, no. 1, pp. 56 - 62, 16 January 2013.

[39] D. Burghoff, T.-Y. Kao, D. Ban, A. W. M. Lee, Q. Hu and J. Reno, "A terahertz pulse emitter monolithically integrated with a quantum cascade laser," *Applied Physics Letters,* vol. 98, no. 6, p. 061112, 2011.

[40] K. Kan, J. Yang, A. Ogata, S. S. T. Kondoh, K. N. I. Nozawa, T. Toigawa, Y. Yoshida, H. Kitahara, K. Takano, M. Hangyo, R. Kuroda and H. Toyokawa, "Radially polarized terahertz waves from a photoconductive antenna with microstructures," *Applied Physics Letters,* vol. 102, no. 22, p. 221118, 2013.

[41] D. Filipovic, S. Gearhart and G. Rebeiz, "Double-slot antennas on extended hemispherical and elliptical silicon dielectric lens," *IEEE Transactions on Microwave Theory and Technique,* vol. 41, no. 10, pp. 1738-1749, 1993.

[42] A. Baryshev, J. Baselmans, A. Freni, G. Gerini, H. Hoevers, A. Iacono and A. Neto, "Progress in Antenna Coupled Kinetic Inductance Detectors," *Terahertz Science and Technology, IEEE Transactions on,* vol. 1, no. 1, pp. 112 - 123, September 2011.

[43] S.-W. Lee, M. S, Sheshadri, V. Jamnejad and R. Mittra, "Refraction at a Curved Dielectric Interface: Geometrical Optics Solution," *IEEE Transactions on Microwave Theory and Techniques,* Vols. MTT-30, no. 1, pp. 12-19, 1982.

[44] D. M. Hailu, I. A. Ehtezazi and S. Safavi-Naeini, "Fast Analysis of Terahertz Integrated Lens Antennas Employing the Spectral Domain Ray Tracing Method," *IEEE Antennas and Wireless Propagation Letters,* vol. 8, pp. 37-39, 2009.

[45] B. Chantraine-Bares, R. Sauleau, L. Le Coq and K. Mahdjoubi, "A new accurate design method for millimeter-wave homogeneous dielectric substrate lens antennas of arbitrary shape," *IEEE Transactions on Antennas and Propagation,* vol. 53, no. 3, pp. 1069-1082, 2005.

[46] D. M. Hailu, I. A. Ehtezazi, M. Neshat, G. S. A. Shaker and S. Naeini, "Hybrid Spectral-Domain Ray Tracing Method for Fast Analysis of Millimeter-Wave and Terahertz-Integrated Antennas," *IEEE Transactions on Terahertz Science and Technology,* vol. 1, no. 2, pp. 425-434, 2011.

[47] Z. Huang, H. P. Chan, H. Park, E. P. Parrott and E. Pickwell-MacPherson, "Fabrication of a metal wire-grid THz polarizer with a low-cost

manufacturing approach," in *37th International Conference on Infrared, Millimeter, and Terahertz Waves (IRMMW-THz)*, 2012.

[48] A. Wojdyla and G. Gallot, "Brewster's angle silicon wafer terahertz linear polarizer," *Optic Express,* vol. 19, no. 15, pp. 14099-14107, 2011.

[49] J. Li and J. Yao, "Controllable terahertz wave attenuator," *Microwave and Optical Technology Letters,* vol. 50, no. 7, pp. 1810-1812, 2008.

[50] LASNIX, 29 January 2013. [Online]. Available: http://www.lasnix.com/datasheets/neutral-density-filter.pdf. [Accessed 29 July 2015].

[51] T. J. Co.. [Online]. Available: http://www.tydexoptics.com/pdf/THz_Attenuators.pdf. [Accessed 29 July 2015].

[52] I. Microtech Instruments, 2012. [Online]. Available: http://mtinstruments.com/2012/Attenuators.pdf. [Accessed 29 July 2015].

[53] B. Rossi, OPTICS, Massachussets: Addison-Wesley Publishing Company, Inc., 1962.

[54] F. T. Ulaby, E. Michielssen and U. Ravaioli, Fundamentals of Applied Electromagnetics, Sixth Edition, PEARSON, 1994.

[55] "HyperPhysics," [Online]. Available: http://hyperphysics.phy-astr.gsu.edu/hbase/phyopt/freseq.html. [Accessed 13 April 2015].

[56] N. Hiromoto, N. Shiba and K. Yamamoto, "Detection of a human hair with polarization-dependent THz-Time Domain Spectroscopy," in *38th International Conference on Infrared, Millimeter, and Terahertz Waves (IRMMW-THz), 2013* , Mainz, Germany, 2013.

[57] P. R. Bevington, Data Reduction and Error Analysis for The Physical Sciences, United States of America: McGraw-Hill Book Company, 1969.

LIST OF PUBLICATION AND ATTENDED CONFERENCES

Journals:

- **Catur Apriono**, Eko Tjipto Rahardjo, Norihisa Hiromoto, "*Ray tracing method with Fresnel's transmission to calculate polarized radiation power distribution focused by a terahertz Silicon lens antenna*", Infrared Physics & Technology, Volume 69, March 2015, Pages 102–106

- **Catur Apriono**, Eko Tjipto Rahardjo, Norihisa Hiromoto,"*A new method for simulating power flow density focused by a Silicon lens antenna irradiated with linearly polarized thz wave*", Makara Journal of Technology, Volume 19, No. 2 August 2015, Pages 59-64

Conferences:

- **Catur Apriono**, Eko Tjipto Rahardjo, Norihisa Hiromoto, "*Geometrical optic and electromagnetic wave analysis on spherical lens antenna for THz detector*", The 74th JSAP (Japan Society of Applied Physics) Autumn Meeting, Kyoto, September 16th, 2013, ISSN : 2301-6043, ISBN : 978-4-86348-370-5

- **Catur Apriono**, Eko Tjipto Rahardjo, Norihisa Hiromoto, "*Investigation of fresnel transmission factor for estimating power density in spherical THz lens antenna*", The 23rd Japan Society of Infrared (JSIR) Symposium, pp. 67-68, Kanagawa, October 31st – November 1st, 2013

- **Catur Apriono**, Eko Tjipto Rahardjo, Norihisa Hiromoto, "*Investigation of power density in THz lens antenna by ray tracing technique and electromagnetic simulation*", The 15th Takayanagi Kenjiro Memorial Symposium, Hamamatsu Campus, Shizuoka University, pp. S4-27-1 – S4-27-4 November 12nd and 13th, 2013

- **Catur Apriono**, Eko Tjipto Rahardjo, Norihisa Hiromoto, "*Investigation of polarized radiation power distribution focused by a THz silicon lens antenna using ray tracing with Fresnel's transmission*", 2014 The 61st JSAP (Japan

Society of Applied Physics) Spring Meeting, Sagamihara-Japan, March 17-20, 2014, ISBN : 978-4-86348-410-8

- **Catur Apriono**, Eko Tjipto Rahardjo, Norihisa Hiromoto, "*Silicon lens antenna for linear array THz antenna detectors*", 2014 The 75th JSAP (Japan Society of Applied Physics) Autumn Meeting, Sapporo Campus, Hokkaido University, Japan, September 17-20, 2014, ISBN : 978-4-86348-444-3

- **Catur Apriono**, Eko Tjipto Rahardjo, Norihisa Hiromoto, "*A new method for simulating the power flow density focused by a silicon lens antenna irradiated with linearly polarized THz wave*", The 2nd International Conference on Nano Electronics Research and Education (ICNERE) 2014, pp. 104-107, Hamamatsu Campus, Shizuoka University, 24-26 November 2014

- **Catur Apriono**, Eko Tjipto Rahardjo, Norihisa Hiromoto, "*Power flow concentration around focus in a silicon lens calculated for polarized terahertz irradiation by ray tracing with Fresnel's transmission*", The 24th Japan Society of Infrared (JSIR) Symposium, pp. 56-67, Osaka Prefecture University, Osaka, Japan, November 27-28, 2014

- **Catur Apriono**, Eko Tjipto Rahardjo, Norihisa Hiromoto, "*Ray tracing method with Fresnel's transmission for a silicon lens antenna irradiated with linearly polarized THz wave*", The Second International Symposium on Frontiers in THz Technology (FTT) 2015, Hamamatsu, Shizuoka, Japan, August 30 – September 2015